Fluorescent peptide highlights micronodules in murine hepatocellular carcinoma models and human *in vitro*

Renwei Jing[1], Xiaoli Zhou[1], Jingwen Zhao[1], Yushuang Wei[2], Bingfeng Zuo[1], Abin You[1], Quan Rao[1], Xianjun Gao[1], Rong Yang[2], Lu Chen[3], Zhen Lu[1], Qibing Zhou[3], Ning Zhang[3]*, HaiFang Yin[1]*

[1]Department of Cell Biology and Key Laboratory of Immune Microenvironment and Disease (Ministry of Education), Tianjin Medical University, Qixiangtai Road, Heping District, Tianjin, 300070, China

[2] Department of Nanomedicine & Biopharmaceuticals, National Engineering Research Center for Nanomedicine, Huazhong University of Science and Technology, Wuhan, 430074, Hubei Province, China.

[3] Department of Genetics & Cancer Institute and Hospital, Tianjin Medical University, Tianjin 300070, China

Key Words: Tumor-targeting peptide, micronodules, hepatocellular carcinoma, surgical navigation

Corresponding authors:

HaiFang Yin or Ning Zhang

Tianjin Medical University

Qixiangtai Road, Heping District, Tianjin, 300070, China

Tel: +86 (0)22 83336537

Fax: +86 (0)22 83336537

Email: haifangyin@tmu.edu.cn or zhangning@tmu.edu.cn

This article has been accepted for publication and undergone full peer review but has not been through the copyediting, typesetting, pagination and proofreading process which may lead to differences between this version and the Version of Record. Please cite this article as doi: 10.1002/hep.29829

Financial support:

This research was supported by National Key R&D Program of China (no.2017YFC1001902), National Natural Science Foundation of China (no. 81501531, 81672124, 81273420, 81671528 and 81372403) and Tianjin Municipal 13th five-year plan (Tianjin Medical University Talent Project).

Abstract

Early detection and clear delineation of microscopic lesions during surgery are critical to the prognosis and survival of patients with hepatocellular carcinoma (HCC), a devastating malignancy without effective treatments except for resection. Tools to specifically identify and differentiate micronodules from normal tissue in HCC patients can have a positive impact on survival. Here, we discovered a peptide that preferentially binds to HCC cells through phage display. Significant accumulation of the fluorescence-labeled peptide in tumor from ectopic and orthotopic HCC mice was observed within 2 h of systemic injection. Contrast between tumor and surrounding liver is up to 6.5-fold and useful contrast lasts for 30 h. Micronodules (0.03 cm in diameter) in liver and lung can clearly be distinguished from normal tissue with this fluorescence-labeled peptide in orthotopic HCC mice and HCC patients. Compared to indocyanine green (ICG), an FDA-approved imaging contrast agent, up to 8.7-fold higher differentiation ratio of tumor-to-fibrosis is achieved with this fluorescence-labeled peptide. Importantly, this peptide enables up to 10-fold differentiation between HCC-to-peritumoral tissue in human tissues and the complete removal of tumor in HCC mice with surgical navigation. No abnormalities in behavior or activity are observed after systemic treatment, indicating the absence of overt toxicity. The peptide is metabolized with a half-life of approximately 4 h in serum. Conclusions: Our findings demonstrate that micronodules can be specifically differentiated with high sensitivity from surrounding tissue with this molecule, opening clinical possibilities for early detection and precise surgery of HCC.

Introduction

Surgical resection remains the main treatment option for hepatocellular carcinoma (HCC), one of the leading malignancies worldwide (1-3). The stage of diagnosis and the degree of tumor removal largely determines post-surgical prognosis. Resection of HCC can be complicated as the tumor is usually detected at a late stage, frequently multinodular and difficult to distinguish from surrounding tissue, thus early detection is a top priority. Although a multitude of diagnostic approaches such as serum biochemical markers, histological examination and non-invasive imaging are used clinically, the sensitivity and specificity can be improved especially for early stage diagnosis (4, 5). Therefore, development of tools to more sensitively and accurately identify HCC nodules can improve diagnosis and surgical outcome and consequently patient survival.

Recently, advances in imaging-based diagnostic modalities such as computed tomography (CT), ultrasound, positron-emission tomography (PET) and magnetic resonance imaging (MRI) make it possible to detect HCC nodules with a diameter of 2 cm accurately. Importantly, the detection of small lesions with a diameter of 0.5-1 cm becomes possible with improved MRI technique (6-9). However, a major limitation to these techniques is their limited spatial resolution and the difficulty of converting two-dimensional information to the three-dimensional clinical practice for guiding surgery. Moreover, it remains challenging to identify and delineate micronodules with diameters less than 0.5 cm with current imaging approaches.

To address this unmet medical need, peptide probes have been developed for cancer imaging. These probes can possess high binding affinity for the target, specific uptake and retention in the target, rapid clearance from non-target tissues, sufficient capillary permeability, relatively high stability and safety (10, 11). The majority of available tumor-targeting peptides are derived from phage display (12-14). These targeting peptides have been developed not only for *in vivo* imaging, but also for targeted delivery of drugs and biologics (15). Although a number of peptides and small molecules have been developed to target HCC (13, 14, 16-18), their ability to detect micronodules and differentiate normal and abnormal liver tissues from tumor can be improved.

In this study, we identified peptides by phage display that preferentially binds to HCC tissues after systemic administration. We performed *in vitro* selection on excised human HCC patient biopsies, which can closely recapitulate clinical features of HCC in patients, rather than human HCC cell lines as reported previously (19-21). High throughput sequencing was employed to increase the resolution of the selection. Candidate peptides were evaluated for their binding affinity and specificity to HCC cells *in vitro* and *in vivo*. Systemic investigation on the capability of candidate peptides to identify and delineate micronodules was performed in ectopic, orthotopic and autochthonous HCC mice. Moreover, we compared the accuracy of this fluorescence-labeled peptide in delineating the margin between tumor and

surrounding tissues and demarcating tumors from abnormal liver to indocyanine green (ICG), an FDA-approved tricarbocyanine dye commonly used as an imaging contrast agent in the clinic (22). Our results demonstrate that this peptide can identify up to 0.03 cm microscopic lesions and delineates clearly the margin between tumor and surrounding tissues and can be employed for surgical navigation.

Materials and Methods

Animals

C57BL/6 wild-type and *BALB/C* nude mice (6-8 weeks old, no gender preference) were used in all experiments (the number used was specified in Figure legends). The experiments were repeated at least three times unless otherwise specified. All animal experiments were carried out in the animal unit of Tianjin Medical University (Tianjin, China) according to procedures authorized and specifically approved by the institutional ethical committee (Permit Number: SYXK 2009-0001). Mice were sacrificed by CO_2 inhalation or cervical dislocation at desired time-points, and tissues were fixed with Bouin's solution (Sigma, St. Louis, MO, US) and embedded with paraffin for immunohistochemical and histological studies.

Cell lines

Murine HCC cell line Hepa1-6 was purchased from Boster Biological Technology Ltd (Wuhan, China) and cultured in DMEM medium with 2 mM Glutamine and 10% fetal bovine serum (FBS) as per manufacturer's instructions. Human HCC cell (HepG2),

breast cancer cell (MDA-MB-231), cervical cancer cell (Hela), kidney cancer cell (CRL-1932) and lung cancer cell (A549) were purchased from ATCC biobank and cultured as per manufacturer's instructions. Human liver cell line H7702 and HCC cell lines including MHCC-LM3, MHCC-97H, SMMC7721 and Bel7402 were purchased from BeNa Culture Collection (Beijing, China), and cultured as per manufacturer's instructions. Briefly, H7702, MHCC-LM3, MHC-97H and SMMC7721 cells were cultured in DMEM medium (Invitrogen, US) containing 2mM Glutamine and 10% FBS. Bel7402 cells were cultured in RPMI-1640 medium supplemented with 10% FBS.

Clinical samples

The combined hepatocellular carcinoma and cholangiocarcinoma patient biopsies used in this study were provided by Tianjin Medical University Cancer Hospital. All patients provided written informed consent for the sample collection. This study was conducted in accordance with Declaration of Helsinki and was approved by the Tianjin Medical University Cancer Hospital Ethics Committee.

Statistical analysis

All data are reported as mean values ± SEM. Statistical differences between different groups were evaluated by SigmaStat (Version 3.5; Systat Software, London, UK), with significance set at $p<0.05$. Both parametric and non-parametric analyses were applied, in which the Mann-Whitney Rank Sum Test (Mann-Whitney U test) was used for samples on a non-normal distribution whereas a two-tailed t test was performed

for samples with a normal distribution, respectively. Sample size was determined by PASS (Power Analysis and Sample Size) (Version 11, NCSS, UT, US).

Results

P47 bears strong HCC-specific binding affinity *in vitro*

A live slice culturing system was adopted for phage display screening to better represent *in situ* HCC environment (23) and we verified that liver slices could survive for 12 h as demonstrated by histological examination (Supporting Fig. S1A), propidium iodide (PI) staining (Supporting Fig. S1B), lactate dehydrogenase (LDH) and ATP activity assays (Supporting Fig. S1C and D). *In vitro* biopanning was carried out with different excised HCC patient biopsies for two rounds to avoid propagation-related preferential enrichment (24) and enrichment of phage clones in each round was observed (Supporting Fig. S2). Phage clones recovered from the second round of biopanning were chosen for next generation sequencing. Five top candidate peptides were selected for evaluation based on relative abundance (Supporting Table S1). To examine the HCC-specific binding affinity *in vitro*, we incubated 5 μM carboxyfluorescein (FAM)-labeled peptides with different human HCC cells and non-cancerous H7702 hepatocytes and washed out unbound peptides. Brighter fluorescence signals were detected in three human HCC lines treated with P47 or P48 peptides than P1, P20 or P46, with LM3 cells showing the strongest fluorescence signals (Fig. 1A). Consistently, FACS analysis of cellular uptake of FAM-labeled peptides indicated that the highest uptake was observed in LM3 cells

with all peptides (Fig. 1B). Interestingly, P46 only showed strong binding affinity with LM3 (Fig. 1B), suggesting that it might be only amenable to a subpopulation of HCC patients. In contrast, P47 showed greater uptake across different human HCC cells and differentiation between HCC and normal liver cells (Fig. 1B). Although stronger uptake was also observed with P48, it showed much less differentiation between HCC and H7702 cells (Fig. 1B). To further investigate the binding affinity of candidate peptides to other tumor cells, we co-incubated FAM-labeled peptides with cervical cancer (Hela), breast cancer (MDA-MB-231), kidney cancer (CRL-1932) and lung cancer cells (A549) under identical conditions. Concordantly, the strongest fluorescence signals were observed in LM3 cells with all peptides, compared with other tumor cells (Fig.1C and D). The peptide-specific binding of Alexa Fluor (AF) 680-labeled P47 to LM3 cells was further confirmed by the gradually decreased fluorescence intensity after the addition of escalating concentrations of free P47 (Supporting Fig. S3A). Notably, P47 predominantly localized in cytoplasm with small amounts scattered in nuclei (Supporting Fig. S3B). These findings indicated that P47 shows strong HCC-specific binding affinity across different human HCC cells with different genetic backgrounds.

P47 demonstrates HCC-targeting property *in vivo*

To investigate whether P47 is capable of targeting HCC tissues specifically *in vivo*, we intravenously administered FAM-labeled P46, P47 and P48 at 25 mg/kg into orthotopic HCC mice, generated by transplantation with tumors derived from

subcutaneous HCC mice inoculated with $5x10^5$ Hepa1-6 cells. The strongest fluorescence signal in orthotopic tumors and the greatest contrast between tumor and liver were observed in P47-treated mice imaged with the small animal imaging system (IVIS) (Fig. 2A). Comparable fluorescence was observed in both liver and tumor from P48-treated mice and P46 did not stain the tumor effectively (Fig. 2A). Quantitative analysis showed a tumor-to-liver contrast ratio of 5.23±0.84 fold with P47 and no contrast with P46 (0.83±0.13 fold) and P48 (1.18±0.15 fold) (Fig. 2B), suggesting that P47 targets HCC specifically *in vivo*. Two other HCC-targeting peptides (A54 and SP94), identified from phage display and used for targeted drug delivery, were assessed with P47 side-by-side under identical conditions (25 mg/kg in orthotopic HCC mice)(13, 16). Consistent with previous reports, A54 and SP94 preferentially homed to tumor tissues with a tumor-to-liver ratio of 1.68±0.28 or 1.96±0.33 fold (Fig. 2C and D), however a lack of clear delineation of the margin between tumor and surrounding liver was observed for both peptides when compared with anatomical images (Fig. 2C). Compared to A54 and SP94, much stronger fluorescence signals in tumors and clearer visualization of the margin between tumor and surrounding liver were observed with P47 (Fig. 2C and D).

AF680-labeled P47 (500 μg/kg) was intravenously administered into orthotopic mice with small tumors (0.42 cm in longitude), generated by transplantation with tumors derived from subcutaneous HCC mice inoculated with $1x10^6$ 97H cells, and a scrambled peptide with identical amino acid composition was tested under identical

conditions. Well-demarcated tumors were identified by P47 and MRI 30 h after injection (Fig. 2E). In contrast, the scramble peptide did not mark the tumor out (Fig. 2E). Similar results were also seen with large tumors (1.2 cm in longitude) (Fig. 2F). These results demonstrate that P47 can be used to identify tumors *in vivo*.

P47 shows specific accumulation and retention in HCC tissues *in vivo*

To monitor the specific uptake and retention of P47 in tissues *in vivo* over time, we generated an ectopic HCC nude mouse model by inoculating $1x10^6$ LM3 cells subcutaneously. AF680-labeled P47 was administered intravenously into ectopic HCC nude mice at 500 μg/kg and mice were examined at different time-points with IVIS. Specific accumulation of P47 in tumor tissues was visible at 1 h and peaked at 6 h after injection and the fluorescence signal lasted for at least 30 h in tumor tissues (Fig. 3A). In clear contrast, there was no specific uptake in tumor tissues with the scramble control, which was rapidly cleared by 6 h after injection (Fig. 3A).To further verify the specific accumulation and retention of P47, we established another two ectopic HCC nude mouse model inoculated with human 97H ($1x10^6$) or Bel7402 HCC cells ($1x10^6$). Similar patterns of specific uptake and retention in tumor tissues were achieved with AF680-labeled P47 in these models (Fig. 3B and C). Importantly, when we systemically administered FAM-labeled P47 into the same ectopic HCC nude mouse model inoculated with 97H, the same observation was reproduced with a tumor-to-liver ratio of 7.89 ± 3.6 fold, indicating that the conjugated moieties do not affect the tissue distribution and targeting specificity of P47 (Supporting Fig. S4).

Consistent with *in vitro* data, there was no or trace amount of uptake of FAM-labeled P47 found in tumor tissues from ectopic breast cancer nude mice, generated by inoculation with $1x10^6$ MDA-MB-231 cells (Supporting Fig. S4), further confirming the HCC-targeting property of P47 *in vivo*. The specific accumulation and retention of P47 was also observed in tumor tissues from ectopic HCC *C57BL/6* mice inoculated with murine Hepa1-6 cells ($5x10^5$) under an identical dosing condition (Fig. 3D). Quantitative analysis of cellular uptake of AF680-labeled P47 in different HCC models confirmed the same uptake and retention pattern achieved across different HCC models with the plateau uptake reached at 6 h after injection (Fig. 3E). These data support the conclusion that P47 shows specific uptake and retention in HCC tissues irrespective of genetic backgrounds.

To investigate the stability of P47 in serum, we co-incubated P47 in 20% serum and measured the integrity of the peptide at different time-points with liquid chromatography-electrospray mass spectrometry (LC-MS). The results indicated that 58.8% of the peptide remained intact at 4 h time-point and small fractions of successive fragments of P47 starting from the N terminus appeared at 1 h after co-incubation, suggesting that the entire peptide had been sequentially degraded from the C terminus (Fig. 3F).

P47 identifies micronodules in liver and lung in orthotopic HCC mice

In orthotopic HCC mice bearing micronodules, AF680-labeled P47 was strikingly

able to highlight diffuse micronodules with a diameter of less than 0.03 cm (Fig. 4A). These micronodules were confirmed by pathological and immunohistochemical staining (Fig. 4B). Moreover, metastatic micronodules (0.04 cm in longitude) in lung were also highlighted by AF680-labeled P47 in orthotopic HCC mice and verified by histological examination (Fig. 4C). These findings underlined the sensitivity and HCC-targeting property of P47 in detecting microscopic lesions in orthotopic HCC mice and demonstrate how P47 can be a surgical aid that can result in much better surgical outcomes after resection.

P47 differentiates HCC from abnormal liver in autochthonous HCC mice

Considering fibrosis frequently occurs concurrently with HCC, clear differentiation between fibrosis and HCC will be of clinical relevance. Therefore we generated a mouse model bearing liver fibrosis induced by CCl_4 prior to the inoculation of human LM3 cells ($1x10^6$) subcutaneously (Supporting Fig. S5A). Specific uptake of AF680-labeled P47 was found in tumor but not in fibrotic liver with a tumor-to-fibrotic liver ratio of 4.44±1.05 fold at 2 h after intravenous injection of AF680-labeled P47 (500 μg/kg) (Supporting Fig. S5B and C). In clear contrast, simultaneously injected ICG (3 mg/kg), a contrast agent used pre-clinically and clinically for HCC imaging (22, 25), showed accumulation both in fibrotic liver and tumor tissues with a tumor-to-fibrotic liver ratio of 1.16±0.16 fold (Supporting Fig. S5B and C). Interestingly, an accumulation of ICG was found in hyperemic areas of ectopic tumor (Supporting Fig. S5D), suggesting that ICG is mainly taken up by

actively metabolizing tumor while P47 seems to bind to HCC independent of metabolic activity. A clear delineation of the margin between fibrotic liver and tumor was observed at 1 h after intravenous injection of AF680-labeled P47, whereas higher uptake was found in fibrotic liver than tumor tissues with ICG (Fig. 5A and Supporting Fig. S5E). Quantitative analysis revealed that an 8.68-fold higher tumor-to-fibrotic liver ratio was achieved with AF680-labeled P47 than ICG (Fig. 5B), indicating that P47 is able to differentiate fibrotic liver from tumor. To investigate the ability of P47 to discriminate abnormal liver and HCC in a clinically relevant setting, we systemically administered AF680-labeled P47 into an autochthonous HCC mouse model established by diethylnitrosamine (DENA) induction as reported previously (26). As expected, specific uptake of AF680-labeled P47 was detected in tumor tissues bearing binuclear cells irrespective of the number (Fig. 5C and D), however ICG was only found in tumor tissues containing fewer binuclear cells, consistent with previous report (27), and regenerative nodules with intact hepatic cords (Fig. 5C and D). Remarkably, lung metastasis was identified by P47 but not by ICG in orthotopic HCC mice (Supporting Fig. S5F). Interestingly, ICG was also absorbed by compressed hepatocytes but not for P47 (Fig. 5D). The accumulation of ICG in abnormal liver was further confirmed in tumor-free mouse models bearing regenerative nodules and ballooning degeneration (Fig. 5E), though the bio-distribution of P47 and ICG was similar in normal *C57BL6* mice at 2 h post-administration (Fig. 5F). These data further strengthen the conclusion that P47 shows stronger HCC-targeting property than ICG and can differentiate abnormal liver from HCC irrespective of the tumor cell

division status. No morphological changes were observed in kidney and liver from mice injected with 50 mg/kg P47, which is 100-fold higher than the required dose for detecting HCC with AF680-labeled P47 (Supporting Fig.S5G), confirming that P47 is safe to use *in vivo*.

P47 discriminates tumors from peritumoral tissues in HCC patients

To evaluate the clinical applicability of P47 in differentiating tumor from abnormal liver in HCC patients, we applied FLAG-tagged P47 to HCC tissue microarrays (Supporting Table S2). Specific staining of FLAG-tagged P47 was detected in HCC tissues but not in corresponding peritumoral and distal tissues (Fig. 6A) and the HCC-to-peritumoral tissue contrast ratio reached up to 9.02-fold in patient No. D19A2424 with a mean value of 4.28±0.96 fold (Fig. 6B). Strikingly, 83.3% of tested HCC tissues showed a HCC-to-peritumor ratio >3 fold (Fig. 6B). Clear delineation of HCC from highly heterogeneous background liver, including fatty degeneration, fibrosis, inflammation and pseudo-lobule formation, was also detected with FLAG-tagged P47 in HCC tissue arrays (Fig. 6C), suggesting that P47 is able to discriminate HCC from heterogeneous peritumoral tissue in the clinic. Further examination on metastatic HCC samples revealed a clear staining of FLAG-tagged P47 in metastatic HCC tissues (Fig. 6D) with a positive rate of 83.3% (10/12), indicating that P47 can detect secondary tumor nodules in HCC patients. To assess whether P47 can identify cholangiocarcinoma, a type of liver cancer with low incidence(28), we examined combined HCC and intrahepatic- cholangiocarcinoma

(ICC) patient tissues. Strikingly, clear staining of P47 was observed in both ICC and HCC tissues with a positive rate of 100% (12/12) and no signal was found in corresponding peritumoral regions and bile ducts (Fig. 6E and F), suggesting that P47 can discriminate both HCC and ICC from abnormal liver. Importantly, the ability of P47 to differentiate between HCC and peritumoral regions increases with the progression of HCC (Supporting Table S2), indicating its clinical potential in surgical resection.

P47 can be used for fluorescence-guided surgical navigation

To investigate whether P47 can be useful for surgical navigation, we injected IRDye800CW (IR800)-labeled P47 (0.5 mg/kg) into ectopic HCC nude mice intravenously. Clear delineation of the margin between tumor and surrounding tissues was observed 24 h after injection and the fluorescence disappeared in mice after surgical excision (Fig. 7A). To quantify the efficacy and completeness of IR800-labeled P47-guided surgery, we used Alu PCR to measure residual human cancer cells remaining in the tumor bed after surgical excision. The quantification of human Alu sequence has been shown to be able to detect the equivalent of one human tumor cell in $1x10^6$ murine cells (29). Residual tumor cells can thus be detected sensitively using human Alu PCR. The results showed that 1000-fold fewer residual tumor cells (normalized DNA content =0.00098$\pm$0.00051, n=3) found in the edge of surgical excision compared to excised human tumor tissues (Fig. 7B), suggesting that the tumor is completely removed. To test the applicability of P47-guided surgical

navigation in orthotopic HCC mice, we intravenously administered the same amount of IR800-labeled P47 into orthotopic HCC mice. Strikingly, IR800-labeled P47 was able to delineate both large tumor and diffused micronodules from surrounding tissues in orthotopic HCC mice (Fig. 7C and D). Quantification of human Alu sequence in residual surrounding tissues after the excision of micronodules revealed the absence of human tumor cells in tissues surrounding the excision (Fig. 7E). Altogether, the data demonstrate that P47 can be useful for fluorescence-guided surgical navigation in HCC.

Discussion

Peptide-based molecular imaging is emerging as one of the main modalities for early detection and surgical navigation of various solid tumors such as mammary adenocarcionma, melanoma, fibrosarcoma and salivary gland cancers (29, 30), however peptides truly capable of outlining microscopic lesions in HCC remain lacking. Here, we demonstrate that a HCC-targeting peptide, identified by phage display in live HCC patient slices, can specifically identify and delineate micronodules with a detection limit of 0.03 cm in liver and metastatic lung. Compared to the commonly used ICG, P47 showed superiority in sensitivity and specificity in identifying micronodules and differentiating tumor from abnormal liver with approximately 9-fold higher differentiation capacity between fibrotic liver and HCC. Importantly, P47 can be used to differentiate HCC and ICC from peritumoral regions in patients with a highest ratio of tumor-to-peritumor up to 10-fold, indicating its

potential in surgical navigation. IR800-labeled P47 enables surgical excision and complete removal of diffused micronodules in ectopic and orthotopic HCC mice. Furthermore, P47 can be readily metabolized with a half-life of 4 h without any overt toxicity at higher dose. To our knowledge, this is the first demonstration showing that a HCC-targeting peptide is capable of identifying 0.03 cm microscopic lesions and guiding surgery in orthotopic HCC mice.

In our study, to maximize the successful rate of identifying clinically applicable peptides, we adopted a live slice culturing system, in which the integrity of tissues and *in situ* environment were maximally preserved, for *in vitro* biopanning (23). We also employed different HCC patient slices for each selection round to capture only surface targets common to different HCCs but not normal liver tissue. It was reported that the rate of false positive hits increases with multiple rounds of repetitious selection due to nonspecific binding to materials such as plastics or amino acid-based propagation-related enrichment (24). Therefore, in the current study, we selected earlier round of enriched phage clones for high throughput sequencing to minimize the false positive hits and to increase the coverage for selected clones. These considerations contribute greatly to the successful identification of this novel HCC-targeting peptide.

The superiority of P47 to clinically used ICG in sensitivity and specificity of detecting HCC was demonstrated in different HCC models. Particularly, the capability of P47 in

differentiating tumors from abnormal liver such as fibrosis, regenerative nodules, ballooning degeneration and compressed hepatocytes, shown in the more clinically relevant DENA-induced autochthonous HCC mice manifesting pathological complexity and heterogeneity, presents great advantages to ICG and also can maximize the preservation of remaining liver functions in HCC patients, which is extremely important for the prognosis. This feature was further confirmed in HCC patient tissue microarrays and in combined HCC and ICC patient biopsies, fully demonstrating its clinical implications in diagnosis and image-guided surgical navigation. The complete removal of diffused micronodules in orthotopic HCC mice with IR800-labeled P47 guided surgical resection further underlines its clinical potential in the application of molecular navigation. It should be noted that there may still be a need to find the optimal timing for P47-guided surgery after administration in clinical trials as the signal to noise ratio clearly varies with time (Figure 3). Interestingly, the ability of P47 in differentiating tumor from peritumoral tissues increases with the progression of HCC i.e. the highest tumor-to-peritumor ratio was detected in stage II-III (Edmonson -Steiner grade) (31) HCC patients, which covers the largest population of HCC patients with definitive diagnosis. Also this observation provides hints for future studies on the identification of P47 receptor. More clinical studies are warranted to confirm the applicability of P47 in all HCCs in future.

Taken together, we develop a novel HCC-targeting peptide with high sensitivity and specificity and demonstrate that this peptide enables identification and surgical

navigation of micronodules in HCC mice and thus provide a promising tool for molecular imaging of HCC in the clinic.

Acknowledgements

The authors thank Dr Yiqi Seow (Biomedical Sciences Institutes, A*STAR, Singapore) for critical review of the manuscript and Drs Wenting Shang and Tianpei Guan (Institute of Automation, Chinese Academy of Sciences, Beijing, China) for the assistance with the surgical navigation.

Author Contributions

R.J. and H.Y conceived and designed the experiments, analyzed the data and wrote the manuscript with input from all authors. R.J., X. Z., J. Z., B. Z., A. Y., Q. R. and Z. L. carried out the experiments. Y. W., R. Y. and Q. Z. performed the synthesis of AF680-labeled peptides. L. C. and N. Z. provided and analyzed clinical samples.

Competing interests

The authors declare competing financial interests and have filed a patent.

References

1. Erstad DJ, Tanabe KK. Hepatocellular carcinoma: early-stage management challenges. J Hepatocell Carcinoma 2017;4:81-92.

2. Margarit C, Escartin A, Castells L, Vargas V, Allende E, Bilbao I. Resection for hepatocellular carcinoma is a good option in Child-Turcotte-Pugh class A patients with cirrhosis who are eligible for liver transplantation. Liver Transpl 2005;11:1242-1251.

3. Belghiti J, Kianmanesh R. Surgical treatment of hepatocellular carcinoma. HPB (Oxford)

2005;7:42-49.

4. Ryder SD, British Society of G. Guidelines for the diagnosis and treatment of hepatocellular carcinoma (HCC) in adults. Gut 2003;52 Suppl 3:iii1-8.

5. Spangenberg HC, Thimme R, Blum HE. Serum markers of hepatocellular carcinoma. Semin Liver Dis 2006;26:385-390.

6. Choi JY, Lee JM, Sirlin CB. CT and MR imaging diagnosis and staging of hepatocellular carcinoma: part I. Development, growth, and spread: key pathologic and imaging aspects. Radiology 2014;272:635-654.

7. Choi JY, Lee JM, Sirlin CB. CT and MR imaging diagnosis and staging of hepatocellular carcinoma: part II. Extracellular agents, hepatobiliary agents, and ancillary imaging features. Radiology 2014;273:30-50.

8. Arif-Tiwari H, Kalb B, Chundru S, Sharma P, Costello J, Guessner RW, Martin DR. MRI of hepatocellular carcinoma: an update of current practices. Diagn Interv Radiol 2014;20:209-221.

9. Lee JM, Yoon JH, Joo I, Woo HS. Recent Advances in CT and MR Imaging for Evaluation of Hepatocellular Carcinoma. Liver Cancer 2012;1:22-40.

10. Lee S, Xie J, Chen X. Peptide-based probes for targeted molecular imaging. Biochemistry 2010;49:1364-1376.

11. Whitney MA, Crisp JL, Nguyen LT, Friedman B, Gross LA, Steinbach P, Tsien RY, et al. Fluorescent peptides highlight peripheral nerves during surgery in mice. Nat Biotechnol 2011;29:352-356.

12. Pasqualini R, Ruoslahti E. Organ targeting in vivo using phage display peptide libraries. Nature 1996;380:364-366.

13. Lo A, Lin CT, Wu HC. Hepatocellular carcinoma cell-specific peptide ligand for targeted drug delivery. Mol Cancer Ther 2008;7:579-589.

14. Situ JQ, Ye YQ, Zhu XL, Yu RS, You J, Yuan H, Hu FQ, et al. Specific targeting of A54 homing peptide-functionalized dextran-g-poly(lactic-co-glycolic acid) micelles to tumor cells. Int J Nanomedicine 2015;10:665-675.

15. Li ZJ, Cho CH. Peptides as targeting probes against tumor vasculature for diagnosis and drug delivery. J Transl Med 2012;10 Suppl 1:S1.

16. Du B, Han H, Wang Z, Kuang L, Wang L, Yu L, Wu M, et al. targeted drug delivery to hepatocarcinoma in vivo by phage-displayed specific binding peptide. Mol Cancer Res 2010;8:135-144.

17. Liu N, Tan Y, Hu Y, Meng T, Wen L, Liu J, Cheng B, et al. A54 Peptide Modified and Redox-Responsive Glucolipid Conjugate Micelles for Intracellular Delivery of Doxorubicin in Hepatocarcinoma Therapy. ACS Appl Mater Interfaces 2016;8:33148-33156.

18. Toita R, Murata M, Tabata S, Abe K, Narahara S, Piao JS, Kang JH, et al. Development of human hepatocellular carcinoma cell-targeted protein cages. Bioconjug Chem 2012;23:1494-1501.

19. Zhu D, Qin Y, Wang J, Zhang L, Zou S, Zhu X, Zhu L. Novel Glypican-3-Binding Peptide for in Vivo Hepatocellular Carcinoma Fluorescent Imaging. Bioconjug Chem 2016;27:831-839.

20. Jia WD, Sun HC, Zhang JB, Xu Y, Qian YB, Pang JZ, Wang L, et al. A novel peptide that selectively binds highly metastatic hepatocellular carcinoma cell surface is related to invasion and metastasis. Cancer Lett 2007;247:234-242.

21. Zhang B, Zhang Y, Wang J, Zhang Y, Chen J, Pan Y, Ren L, et al. Screening and identification of a targeting peptide to hepatocarcinoma from a phage display peptide library. Mol Med 2007;13:246-254.

22. Kaibori M, Matsui K, Ishizaki M, Iida H, Sakaguchi T, Tsuda T, Okumura T, et al. Evaluation of fluorescence imaging with indocyanine green in hepatocellular carcinoma. Cancer Imaging 2016;16:6.

23. de Graaf IA, Olinga P, de Jager MH, Merema MT, de Kanter R, van de Kerkhof EG, Groothuis GM. Preparation and incubation of precision-cut liver and intestinal slices for application in drug metabolism and toxicity studies. Nat Protoc 2010;5:1540-1551.

24. t Hoen PA, Jirka SM, Ten Broeke BR, Schultes EA, Aguilera B, Pang KH, Heemskerk H, et al. Phage display screening without repetitious selection rounds. Anal Biochem 2012;421:622-631.

25. Andreou C, Neuschmelting V, Tschaharganeh DF, Huang CH, Oseledchyk A, Iacono P, Karabeber H, et al. Imaging of Liver Tumors Using Surface-Enhanced Raman Scattering Nanoparticles. ACS Nano 2016;10:5015-5026.

26. Lu Z, Zuo B, Jing R, Gao X, Rao Q, Liu Z, Qi H, et al. Dendritic cell-derived exosomes elicit tumor regression in autochthonous hepatocellular carcinoma mouse models. J Hepatol 2017.

27. Ishizawa T, Fukushima N, Shibahara J, Masuda K, Tamura S, Aoki T, Hasegawa K, et al. Real-time identification of liver cancers by using indocyanine green fluorescent imaging. Cancer 2009;115:2491-2504.

28. Landis SH, Murray T, Bolden S, Wingo PA. Cancer statistics, 1998. CA Cancer J Clin 1998;48:6-29.

29. Nguyen QT, Olson ES, Aguilera TA, Jiang T, Scadeng M, Ellies LG, Tsien RY. Surgery with molecular fluorescence imaging using activatable cell-penetrating peptides decreases residual cancer and improves survival. Proc Natl Acad Sci U S A 2010;107:4317-4322.

30. Hussain T, Savariar EN, Diaz-Perez JA, Messer K, Pu M, Tsien RY, Nguyen QT. Surgical molecular navigation with ratiometric activatable cell penetrating peptide for intraoperative identification and resection of small salivary gland cancers. Head Neck 2016;38:715-723.

31. Nam SW, Park JY, Ramasamy A, Shevade S, Islam A, Long PM, Park CK, et al. Molecular changes from dysplastic nodule to hepatocellular carcinoma through gene expression profiling. Hepatology 2005;42:809-818.

Figure legends

Figure 1. *In vitro* validation of candidate peptides. FAM-labeled candidate peptides (5 μM) were co-incubated with cells ($1x10^4$) and images were taken 6 h later. (**A**) Cellular uptake of FAM-labeled candidate peptides in H7702, SMMC7721, HepG2 and MHCC-LM3 cells. NC（Negative Control）means cells without peptides (scale bar=100 μm). (**B**) Flow cytometry analysis of cellular uptake of candidate peptides in H7702, SMMC7721, HepG2 and MHCC-LM3 cells. (**C**) Cellular uptake of FAM-labeled candidate peptides in MHCC-LM3, Hela, MDA-MB-231, CRL-1932 and A549 cells (scale bar=100 μm). (**D**) Flow cytometry analysis of cellular uptake of candidate peptides in MHCC-LM3, Hela, MDA-MB-231, CRL-1932 and A549 cells (n=3, repeated for 3 times).

Figure 2. *In vivo* verification of candidate peptides. Orthotopic HCC mice were intravenously administered with FAM-labeled peptides at the dose of 25 mg/kg for one single injection. Tissues were harvested, perfused and imaged with IVIS system 2 h after injection. (**A**) Tissue distribution of FAM-labeled P46, P47 and P48 peptides in orthotopic *C57BL/6* HCC mice. S-spleen; K-kidney; H-heart; BF- bright field. (**B**) Quantitative analysis of the tumor/liver ratio of mice injected with P46, P47 or P48 peptides (n=3, error bars are $\pm$ SEM; two-tailed t test, **P<0.01). (**C**) Tissue distribution of FAM-labeled A54, P47 and SP94 peptides in orthotopic *C57BL/6* HCC mice. Q-quadriceps; B-brain. (**D**) Quantitative analysis of the tumor/liver ratio of mice injected with A54 (n=6), P47 (n=4) or SP94 peptide (n=4) (error bars are $\pm$ SEM;

two-tailed t test, **P<0.01). (**E**) Detection of fluorescence signals in AF680-labeled P47- or scrambled peptide (SC) -treated *BALB/C* nude mice bearing small MHCC-LM3 tumor or (**F**) large MHCC-97H tumor generated by transplantation of tumor from subcutaneous HCC mice. Both images in (**F**) represent the same mouse with different views. The arrowhead points to normal liver tissue beneath tumors in orthotopic HCC mice and less fluorescence in normal liver beneath tumors than surrounding tumor tissue was detected.

Figure 3. Real-time monitoring of AF680-labeled P47 peptide in subcutaneous HCC mice. AF680-labeled P47 was administered intravenously into subcutaneous HCC mice at the dose of 500 μg/kg for one single injection. Detection of fluorescence signals in AF680-labeled P47- or scrambled peptide-injected subcutaneous HCC mice bearing MHCC-LM3 (**A**), MHCC-97H (**B**), Bel7402 (**C**) or Hepa1-6 (**D**) tumors at different time-points. BF-bright field. (**E**) Quantitative analysis of fluorescence signal intensity in subcutaneous HCC tumors at different time-points (n=2, the experiment was repeated for 3 times). (**F**) Liquid chromatography-mass spectrometry (LC-MS) analysis of P47 stability in serum.

Figure 4. Investigation on HCC-targeting specificity and sensitivity of AF680-labeled P47 peptide in orthotopic HCC mice bearing micronodules. (**A**) Detection of fluorescence signals in AF680-labeled P47- or scrambled peptide-treated *BALB/C* nude mice bearing diffused MHCC-LM3 micronodules (white bar=2mm to

show the size of micronodules) with IVIS. The arrowheads point to the micronodules. (**B**) Pathological and immunohistochemical analysis of diffused micronodules in orthotopic MHCC-LM3 HCC mice. FLAG-tagged P47 was probed with FLAG antibody and used for immunohistochemistry (scale bar =100 μm). (**C**) Identification of metastatic HCC micronodules in lung with AF680-labeled P47 from orthotopic MHCC-LM3 HCC mice. White arrowheads point micronodules in lung (white bar (=2 mm) was used for showing the size of micronodules). Black arrowheads point to micronodules in the lung in bright field. A' represents the pathological analysis of micronodules in lung (scale bar =100 μm).

Figure 5. Evaluation of AF680-labeled P47 peptide in differentiating HCC from abnormal liver in orthotopic and autochthonous HCC mice. Tissues were harvested and imaged at 2 h or 24 h for AF680-labeled P47 or ICG post-injection, respectively. (**A**) Fluorescence signal distribution of AF680-labeled P47 and ICG in orthotopic *C57BL/6* HCC mice bearing liver fibrosis. Liver fibrosis was induced by CCl_4 prior to tissue implantation of subcutaneous Hepa1-6 tumor. White arrowhead points to tumors; black arrowhead refers to fibrotic liver. (**B**) Quantitative analysis of fluorescence signal intensity in tumor and fibrotic liver. The data was presented as tumor/fibrotic liver ratio for AF680-labeled P47 and ICG after normalization to the background florescence (error bars are $\pm$ SEM). (**C**) Fluorescence signal distribution of AF680-labeled P47 and ICG in DENA-induced autochthonous HCC mice. Wide black arrowhead (B') points to regenerative nodules (RD); A' refers to tumor in

which narrow black arrows point to binuclear tumor cells. (**D**) Fluorescence signal distribution of AF680-labeled P47 and ICG in DENA-induced autochthonous HCC mice with more binuclear tumor cells. White arrow points to the regenerative nodule (RD) (A'); Tu –Tumor. B' and D' refer to areas containing more compressed liver cells with elongated and flat shapes. Wide black arrowheads point to compressed liver cells. C' represents the HCC tumor in which narrow black arrows point to binuclear tumor cells. (**E**) Fluorescence signal distribution of AF680-labeled P47 and ICG in DENA-induced mice bearing hepatic hyperplasia. A' refers to areas with ballooning degeneration; B' represents regenerative nodules (RD). (**F**) Tissue distribution of FAM-labeled P47 and ICG in normal *C57BL/6* mice 2 h post-administration (n=3; error bars are ± SEM). B-brain; Q-quadriceps; Lu- lung; S-spleen; K-kidney; H-heart.

Figure 6. Investigation on the capability of P47 in differentiating HCC from peritumoral regions in HCC patient tissues. (**A**) Immunohistochemical staining of FLAG-tagged P47 in HCC patient tissue arrays. Distal – distal region. FLAG antibody was used to detect the distribution of FLAG-tagged P47 in different HCC patient tissues. D19A2425 and D19A2424 refer to the code for patient tissues. (**B**) Quantitative analysis of staining signal intensity in different HCC patient tissues and percentage of HCC patients with different Tu/P ratios. The data was presented as MIOD (Mean Integrated Optical Density) after normalized to peritumoral tissues (HCC, n=102; peritumoral tissue, n=102; distal region, n=30; error bars are ± SEM). Tu/P refers to Tumor/ peritumoral regions. (**C**) Immunohistochemical staining of

FLAG-tagged P47 in HCC patient tissues containing heterogeneous background liver. In (i) the arrowhead points to inflammation; (ii) arrowheads point to fatty degeneration areas; (iii) liver fibrosis. (**D**) Immunohistochemical staining of FLAG-tagged P47 in HCC patient tissues containing metastasis. (**E**) Immunohistochemical staining of FLAG-tagged P47 in combined HCC and intrahepatic-cholangiocarcinoma (ICC) patient tissues (scale bar=100 μm). The arrowheads point to the margin between tumor and peri-tumor. (**F**) Quantitative analysis of staining signal intensity in different HCC and ICC patient tissues. The data was presented as MIOD after normalized to peritumoral tissues (HCC, n=12; ICC, n=10; peritumoral tissues, n=12; error bars are ± SEM).

Figure 7. Assessment of IR800-labeled P47 peptide in fluorescence-guided surgery. IR800-labeled P47 (0.5 mg/kg) was injected intravenously into ectopic or orthotopic LM3 HCC mice 24 h prior to surgery. (**A**) IR800-labeled P47 guided surgery in ectopic HCC mice. A' and D' show the tumor prior to surgery; B' and E' refer to the tumor during surgery; C' and F' indicate the tumor after surgery. White arrowhead points to the ectopic tumor. (**B**) Quantitative analysis of residual human DNA content with real-time quantitative PCR to verify the completeness of surgery (n=3; error bars are ± SEM). (**C**) IR800-labeled P47 guided surgery in orthotopic HepG2 HCC mice bearing focal and solitary tumors. A' and C' show the tumor prior to surgery; B' and D' indicate the tumor after surgery. White arrowhead points to the orthotopic tumor. (**D**) IR800-labeled P47 guided surgery in orthotopic LM3 HCC

mice bearing multinodular and dispersed micronodules. A' and C' show the tumor prior to surgery; B' and D' indicate the tumor after surgery. White arrowhead points to the orthotopic tumor. (**E**) Quantitative analysis of residual human DNA content with real-time quantitative PCR to verify the complete removal of micronodules (n=3; error bars are ± SEM).

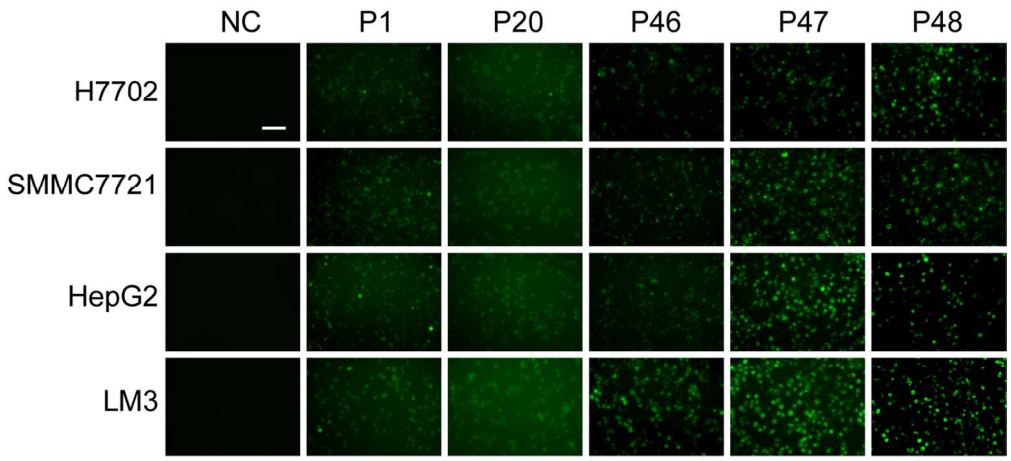

Figure 1. In vitro validation of candidate peptides. FAM-labeled candidate peptides (5 μM) were co-incubated with cells (1x104) and images were taken 6 h later. (A) Cellular uptake of FAM-labeled candidate peptides in H7702, SMMC7721, HepG2 and MHCC-LM3 cells. NC （Negative Control）means cells without peptides (scale bar=100 μm).

122x54mm (300 x 300 DPI)

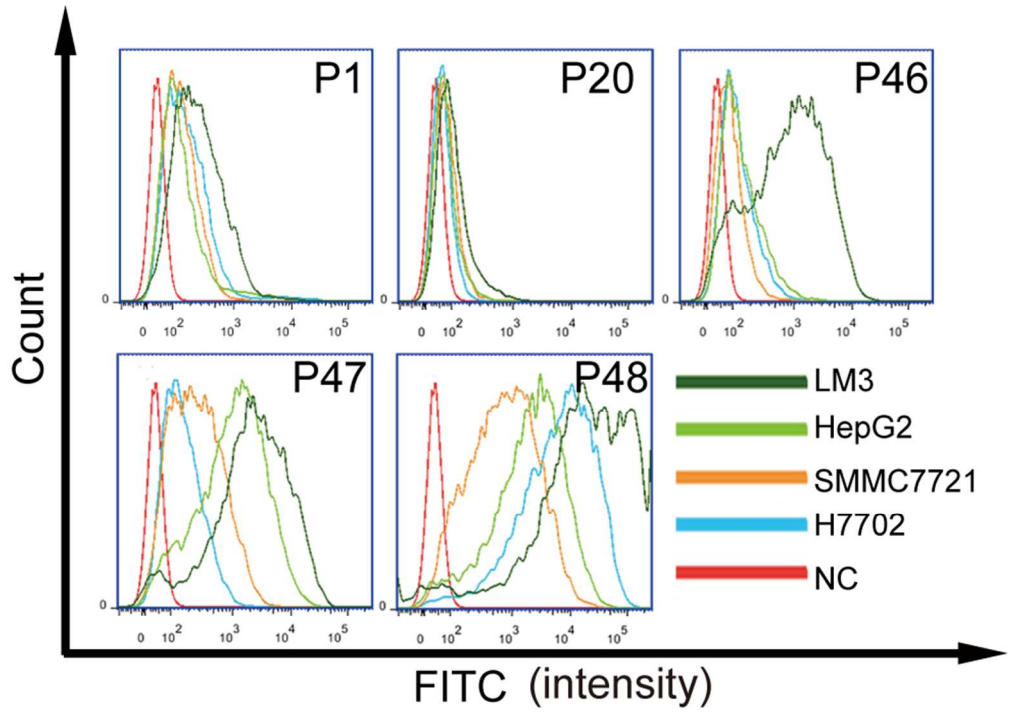

(B) Flow cytometry analysis of cellular uptake of candidate peptides in H7702, SMMC7721, HepG2 and MHCC-LM3 cells.

83x58mm (300 x 300 DPI)

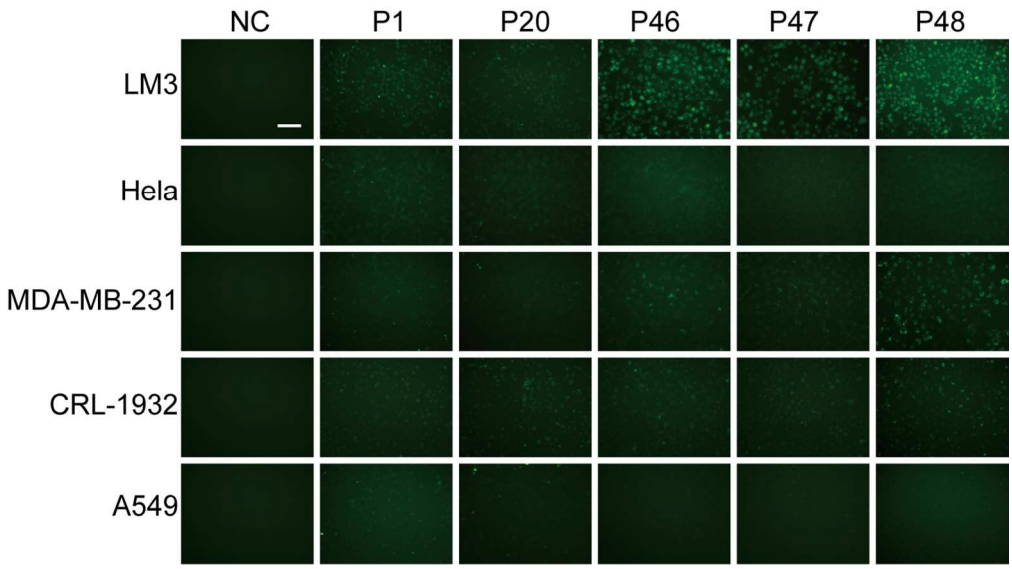

(C) Cellular uptake of FAM-labeled candidate peptides in MHCC-LM3, Hela, MDA-MB-231, CRL-1932 and A549 cells (scale bar=100 μm).

124x69mm (300 x 300 DPI)

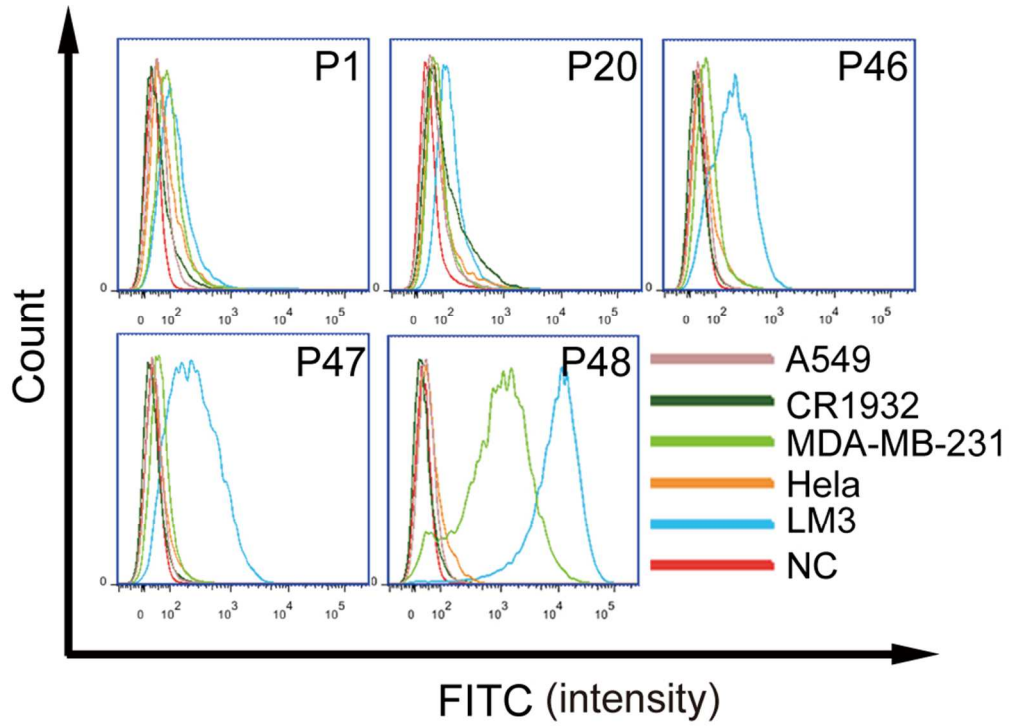

(D) Flow cytometry analysis of cellular uptake of candidate peptides in MHCC-LM3, Hela, MDA-MB-231, CRL-1932 and A549 cells (n=3, repeated for 3 times).

87x63mm (300 x 300 DPI)

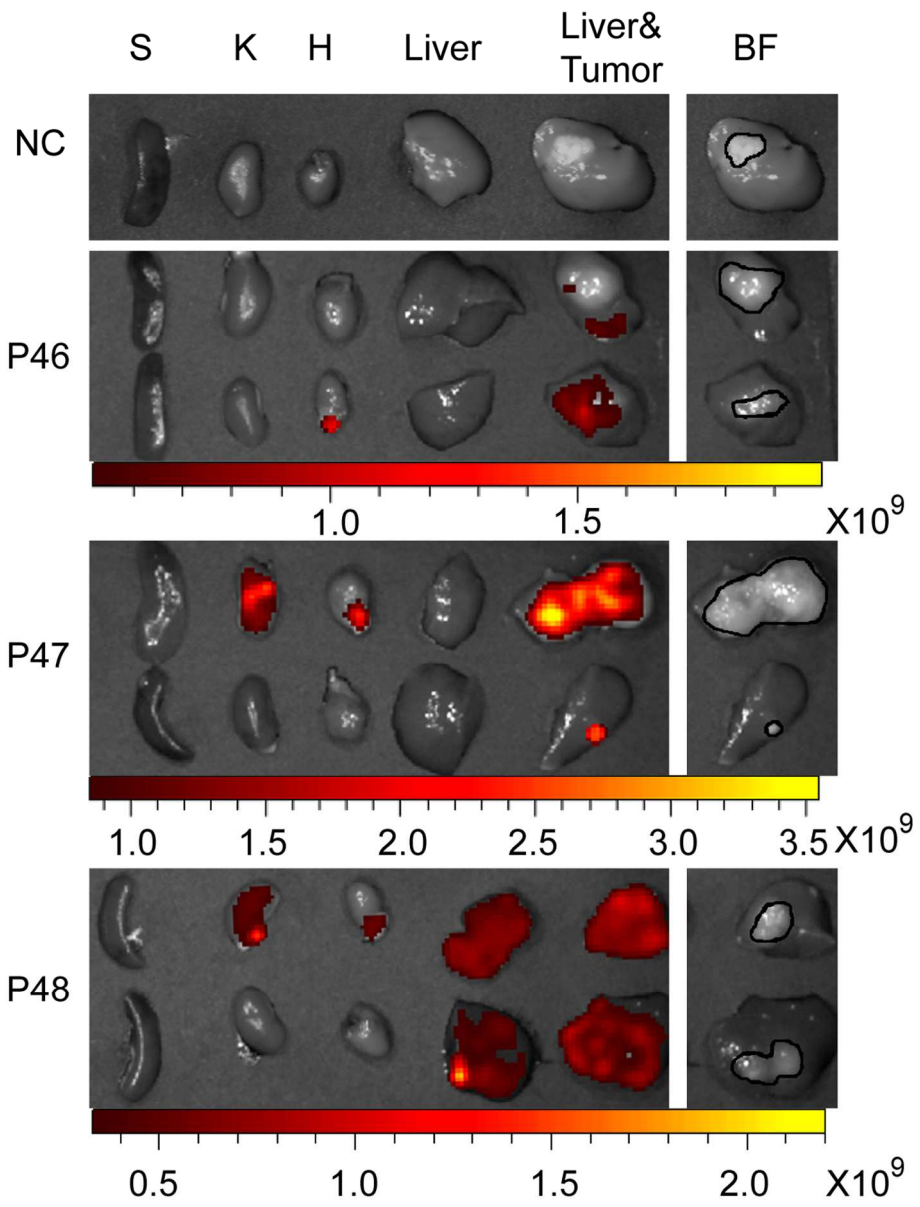

Figure 2. In vivo verification of candidate peptides. Orthoptopic HCC mice were intravenously administered with FAM-labeled peptides at the dose of 25 mg/kg for one single injection. Tissues were harvested, perfused and imaged with IVIS system 2 h after injection. (A) Tissue distribution of FAM-labeled P46, P47 and P48 peptides in orthotopic C57BL/6 HCC mice. S-spleen; K-kideny; H-heart; BF- bright field.

106x141mm (300 x 300 DPI)

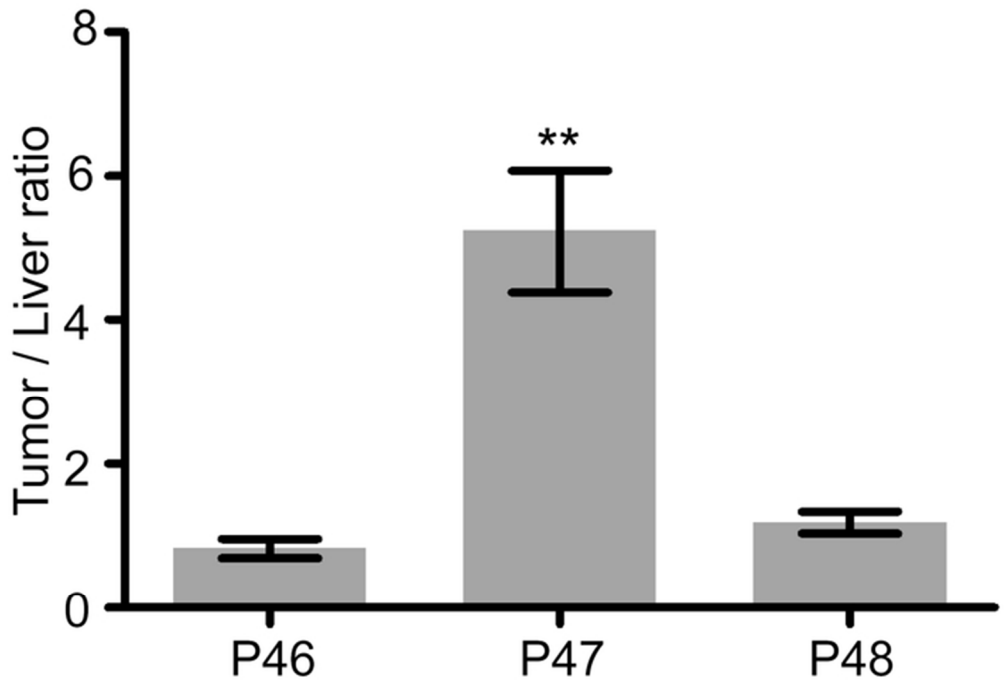

(B) Quantitative analysis of the tumor/liver ratio of mice injected with P46, P47 or P48 peptides (n=3, two-tailed t test, **P<0.01).

60x41mm (300 x 300 DPI)

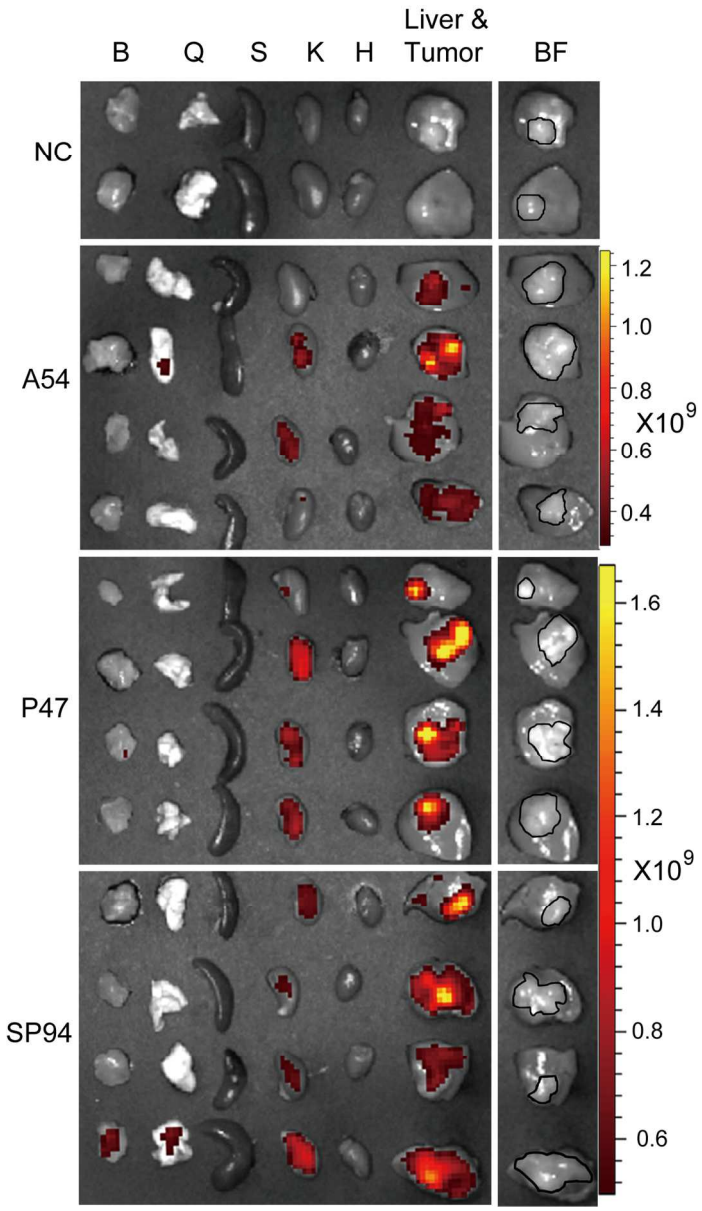

(C) Tissue distribution of FAM-labeled A54, P47 and SP94 peptides in orthotopic C57BL/6 HCC mice. Q-quadriceps; B-brain.

107x186mm (300 x 300 DPI)

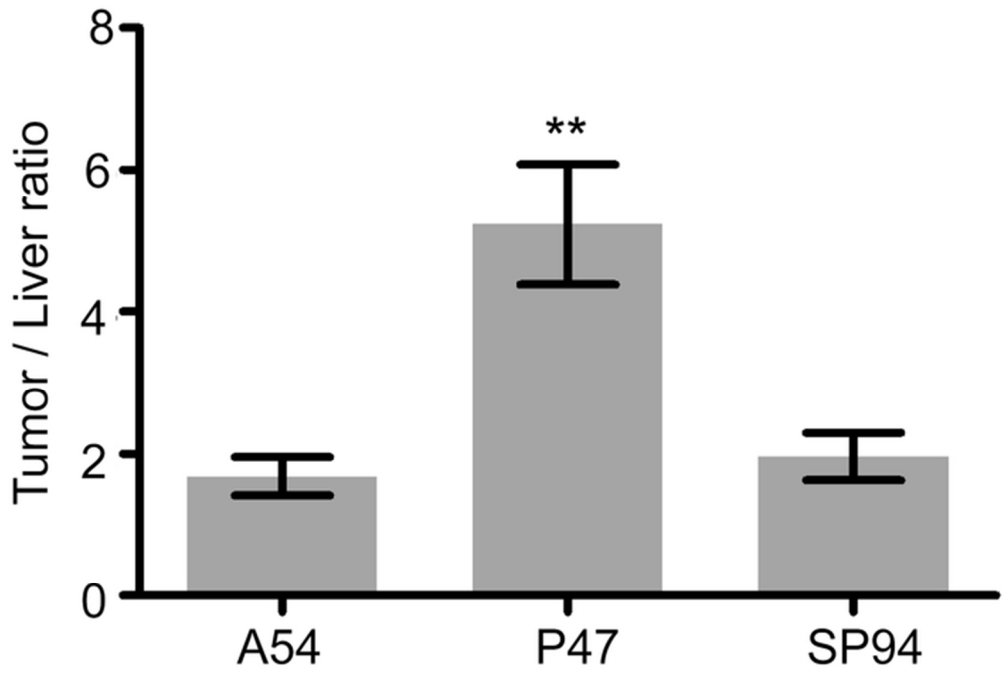

(D) Quantitative analysis of the tumor/liver ratio of mice injected with A54 (n=6), P47 (n=4) or SP94 peptide (n=4) (two-tailed t test, **P<0.01).

59x40mm (300 x 300 DPI)

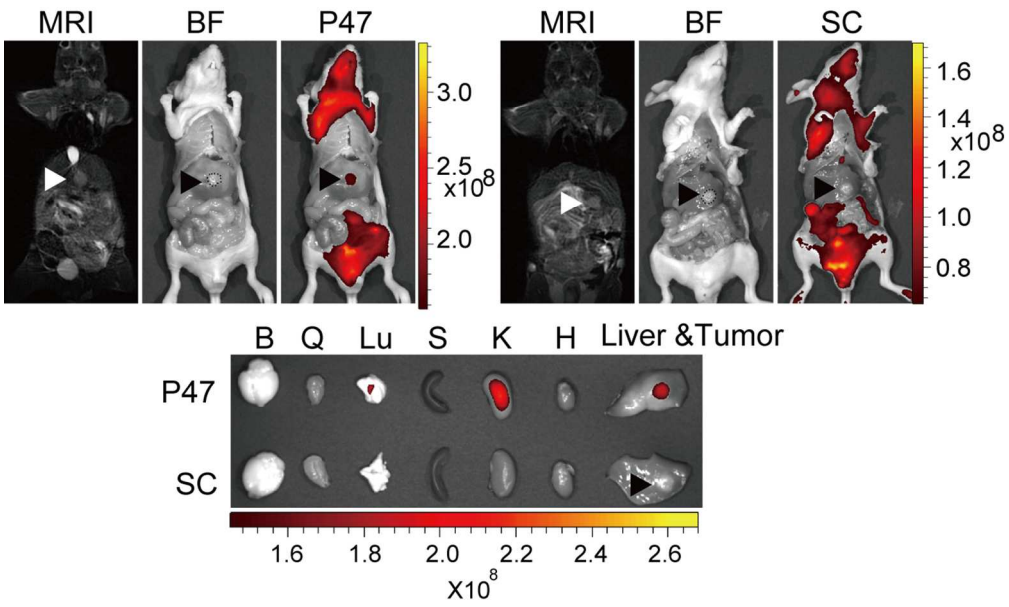

(E) Detection of fluorescence signals in AF680-labeled P47- or scrambled peptide (SC) -treated BALB/C nude mice bearing small MHCC-LM3 tumor or

117x70mm (300 x 300 DPI)

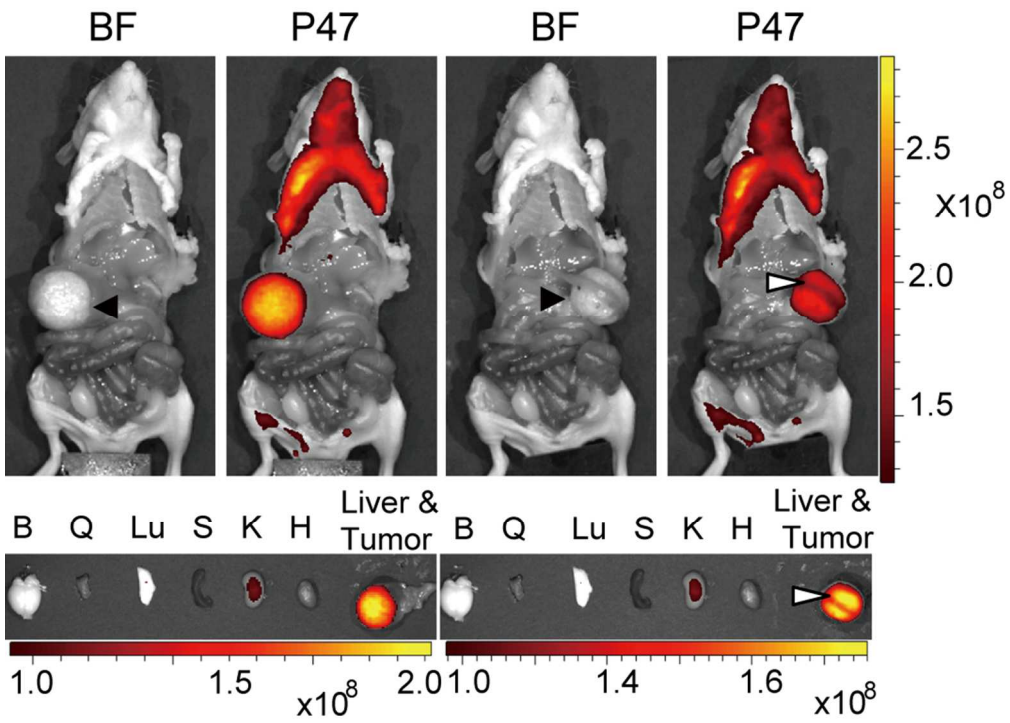

Detection of fluorescence signals in AF680-labeled P47- or scrambled peptide (SC) -treated BALB/C nude mice(F) large MHCC-97H tumor generated by transplantation of tumor from subcutaneous HCC mice. Both images in (F) represent the same mouse with different views. The arrowhead points to normal liver tissue beneath tumors in orthotopic HCC mice and less fluorescence in normal liver beneath tumors than surrounding tumor tissue was detected.

90x65mm (300 x 300 DPI)

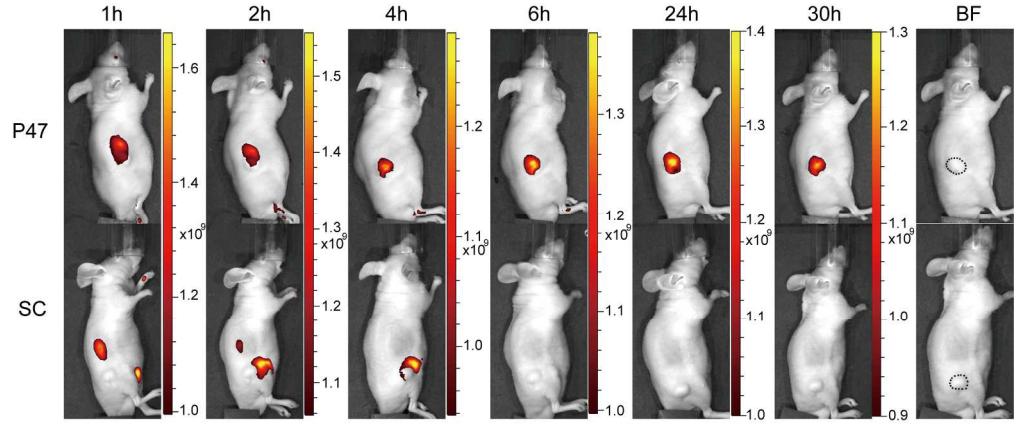

Figure 3. Real-time monitoring of AF680-labeled P47 peptide in subcutaneous HCC mice. AF680-labeled P47 was administered intravenously into subcutaneous HCC mice at the dose of 500 μg/kg for one single injection. Detection of fluorescence signals in AF680-labeled P47- or scrambled peptide-injected subcutaneous HCC mice bearing MHCC-LM3 (A)

206x86mm (300 x 300 DPI)

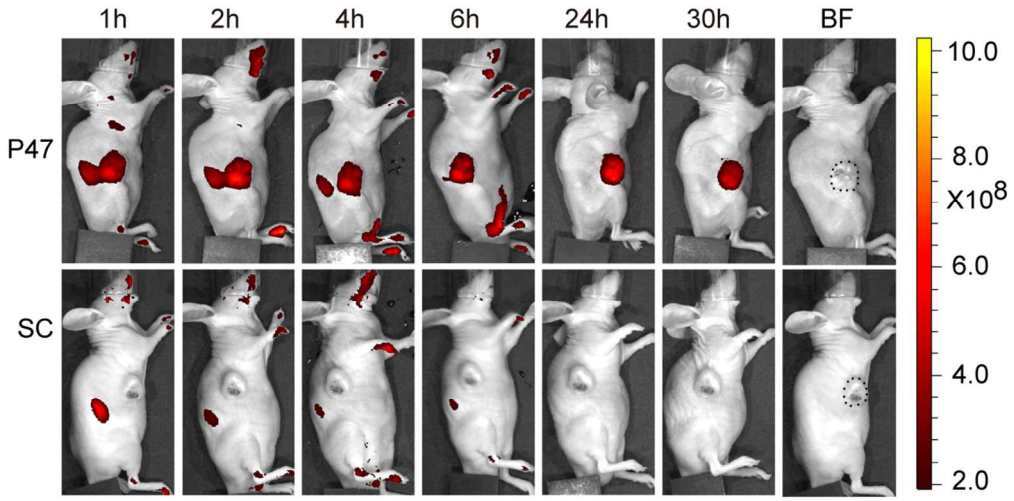

Detection of fluorescence signals in AF680-labeled P47- or scrambled peptide-injected subcutaneous HCC mice bearing MHCC-97H (B) tumors at different time-points.

106x52mm (300 x 300 DPI)

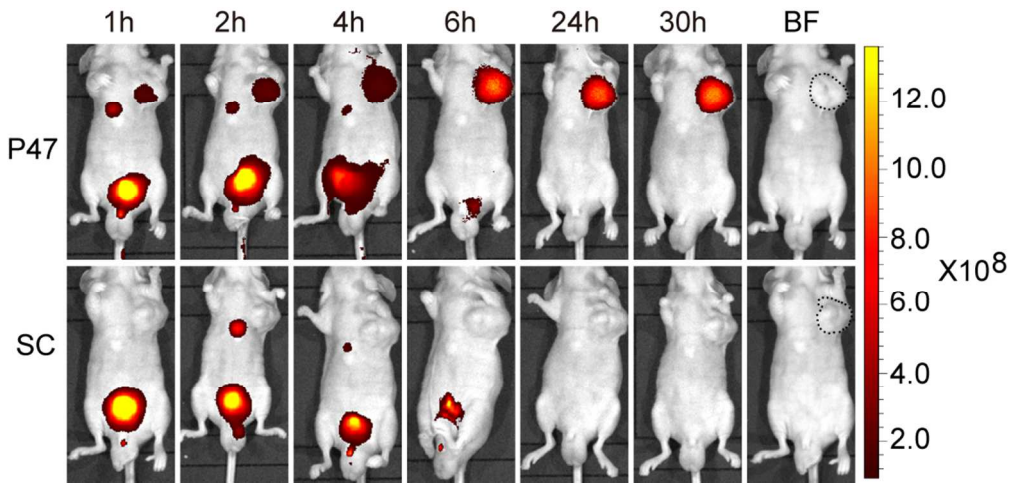

Detection of fluorescence signals in AF680-labeled P47- or scrambled peptide-injected subcutaneous HCC mice bearing Bel7402 (C) tumors at different time-points.

97x46mm (300 x 300 DPI)

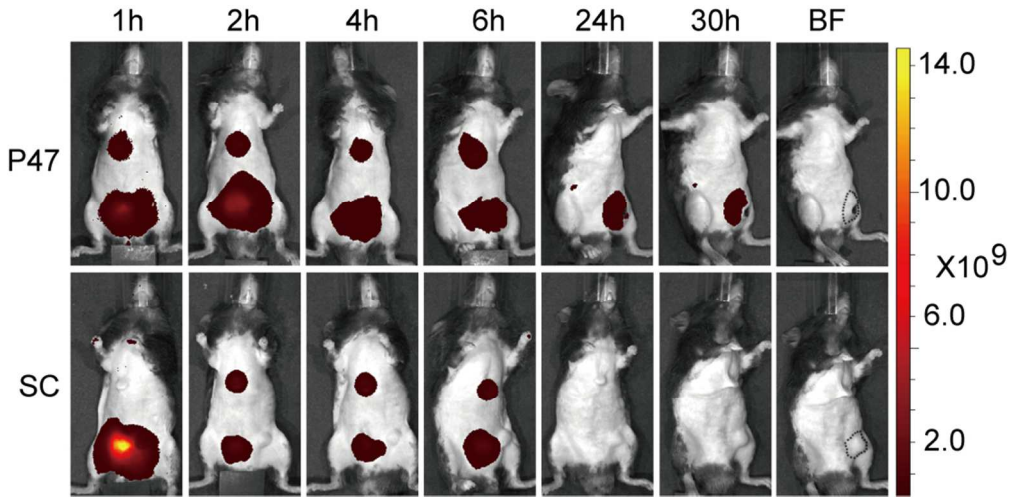

Detection of fluorescence signals in AF680-labeled P47- or scrambled peptide-injected subcutaneous HCC mice bearing Hepa1-6 (D) tumors at different time-points. BF-bright field.

93x46mm (300 x 300 DPI)

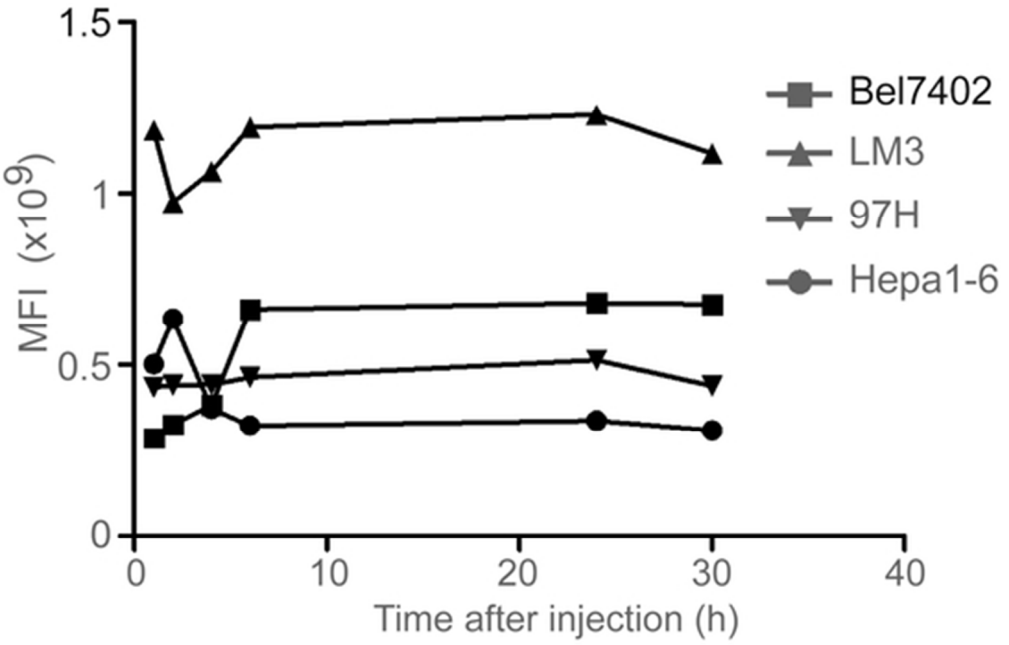

(E) Quantitative analysis of fluorescence signal intensity in subcutaneous HCC tumors at different time-points (n=2, the experiment was repeated for 3 times).

45x29mm (300 x 300 DPI)

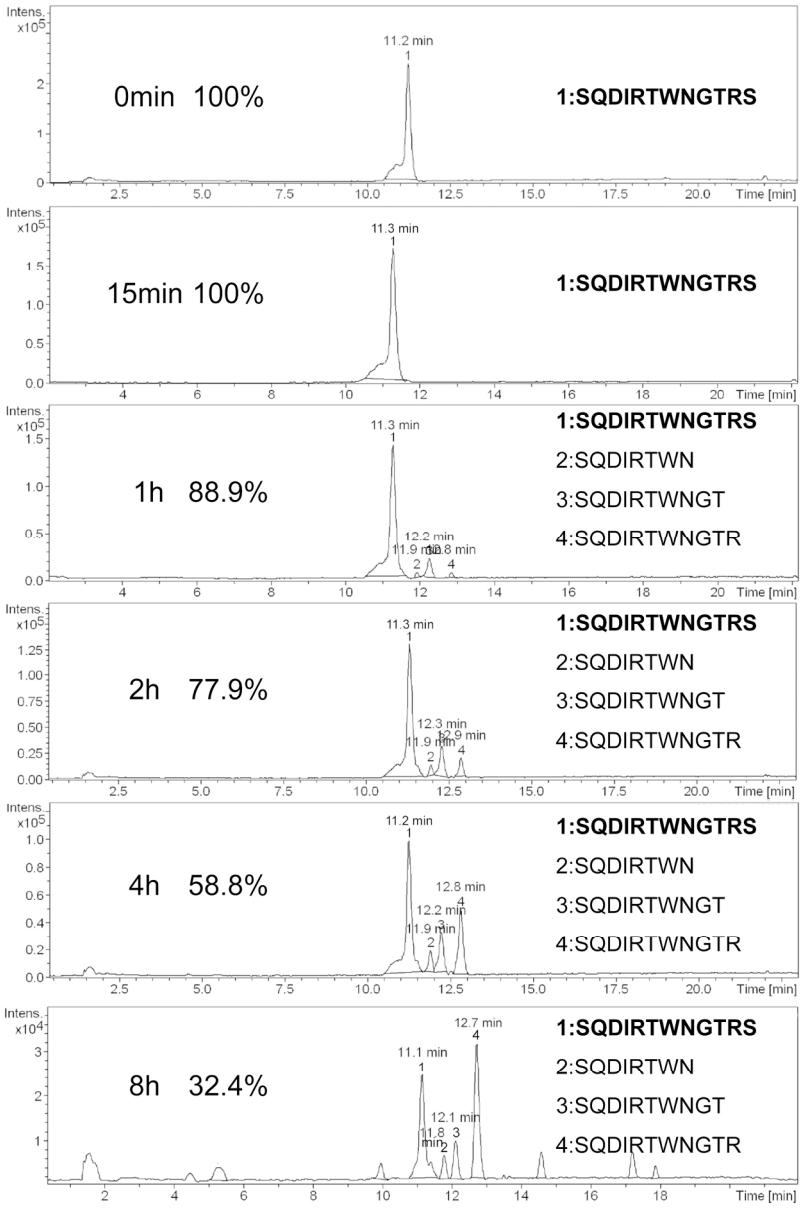

(F) Liquid chromatography-mass spectrometry (LC-MS) analysis of P47 stability in serum.

153x230mm (300 x 300 DPI)

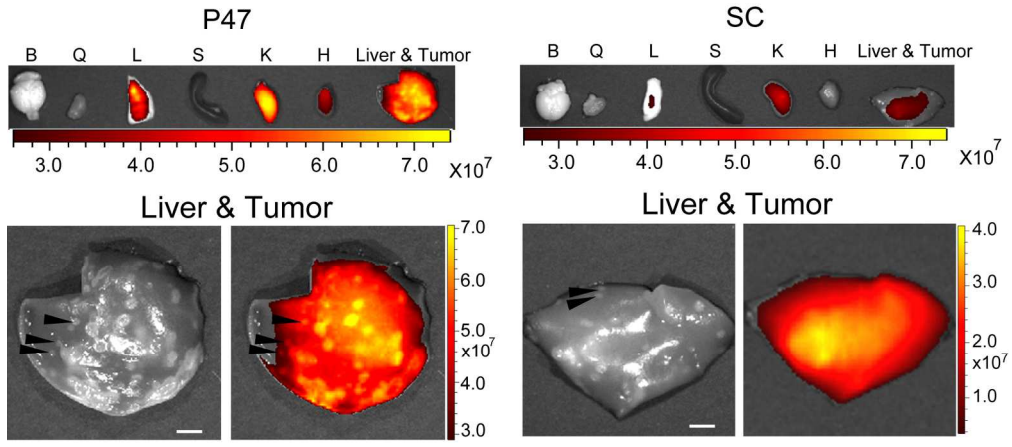

Figure 4. Investigation on HCC-targeting specificity and sensitivity of AF680-labeled P47 peptide in orthotopic HCC mice bearing micronodules. (A) Detection of fluorescence signals in AF680-labeled P47- or scrambled peptide-treated BALB/C nude mice bearing diffused MHCC-LM3 micronodules (white bar=2mm to show the size of micronodules) with IVIS.

181x79mm (300 x 300 DPI)

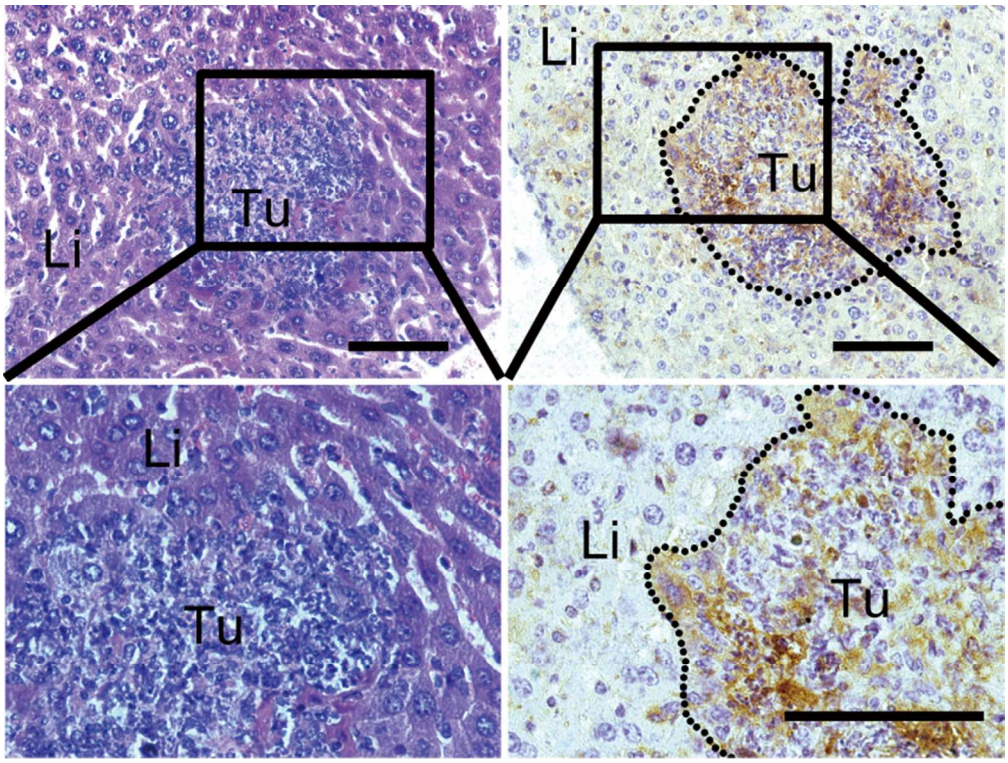

(B) Pathological and immunohistochemical analysis of diffused micronodules in orthotopic MHCC-LM3 HCC mice. FLAG-tagged P47 was probed with FLAG antibody and used for immunohistochemistry (scale bar =100 μm).

71x54mm (300 x 300 DPI)

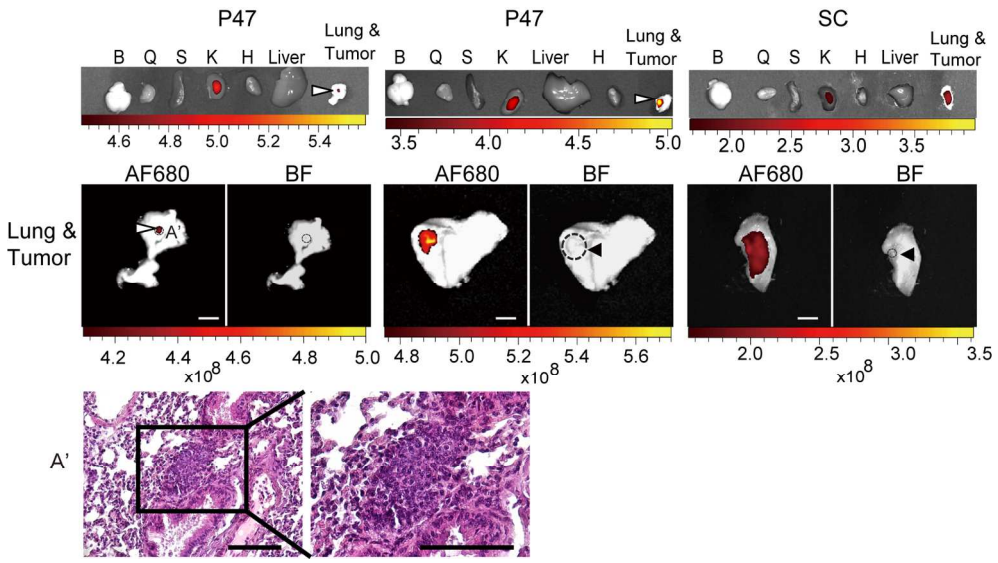

(C) Identification of metastatic HCC micronodules in lung with AF680-labeled P47 from orthotopic MHCC-LM3 HCC mice. White arrowheads point micronodules in lung (white bar (=2 mm) was used for showing the size of micronodules). Black arrowheads point to micronodules in the lung in bright field. A' represents the pathological analysis of micronodules in lung (scale bar =100 μm).

159x88mm (300 x 300 DPI)

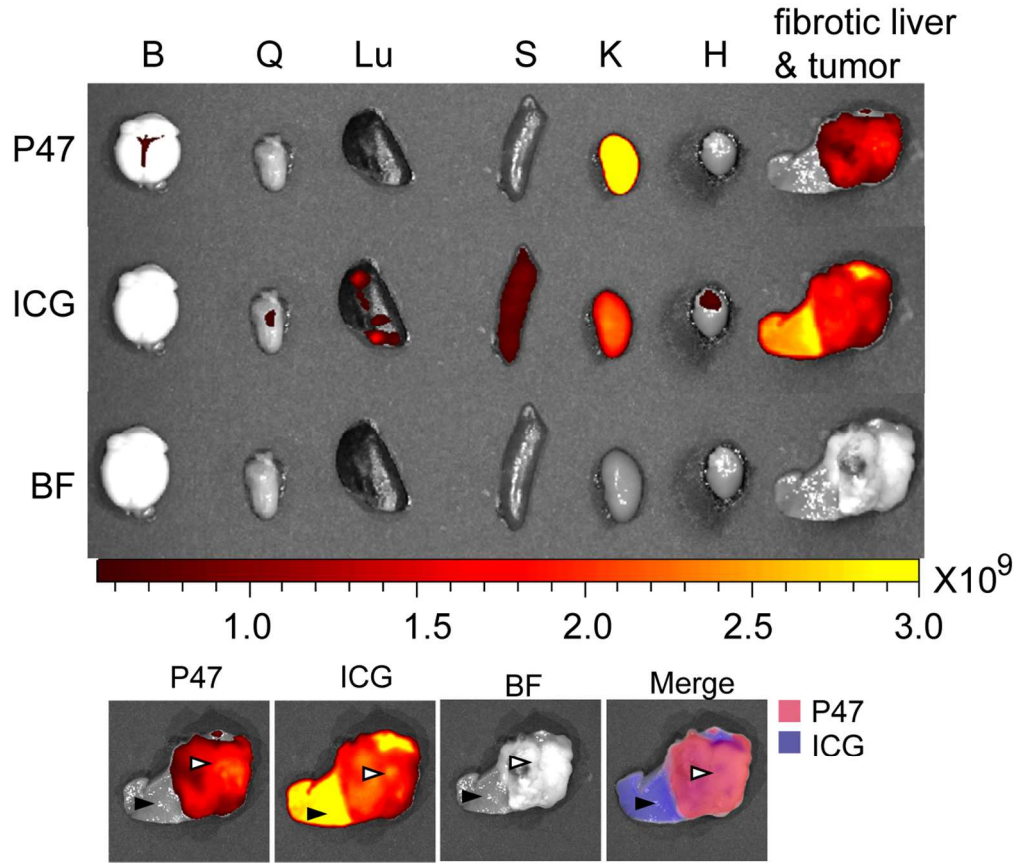

Figure 5. Evaluation of AF680-labeled P47 peptide in differentiating HCC from abnormal liver in orthotopic and autochthonous HCC mice. Tissues were harvested and imaged at 2 h or 24 h for AF680-labeled P47 or ICG post-injection, respectively. (A) Fluorescence signal distribution of AF680-labeled P47 and ICG in orthotopic C57BL/6 HCC mice bearing liver fibrosis. Liver fibrosis was induced by CCl4 prior to tissue implantation of subcutaneous Hepa1-6 tumor. White arrowhead points to tumors; black arrowhead refers to fibrotic liver.

117x100mm (300 x 300 DPI)

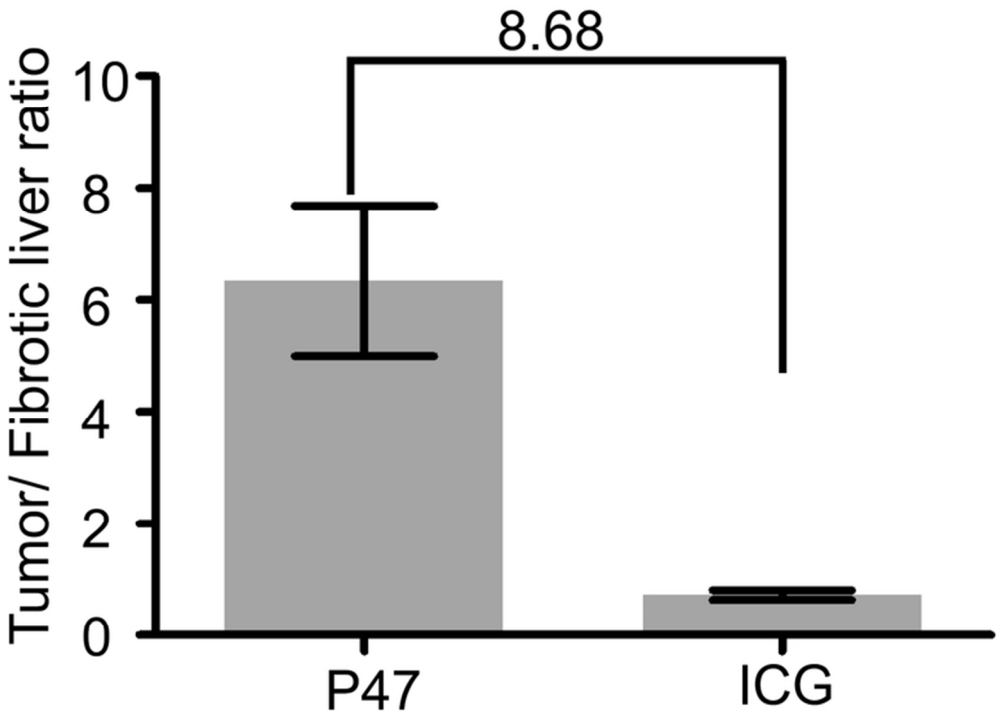

(B) Quantitative analysis of fluorescence signal intensity in tumor and fibrotic liver. The data was presented as tumor/fibrotic liver ratio for AF680-labeled P47 and ICG after normalization to the background florescence.

65x47mm (300 x 300 DPI)

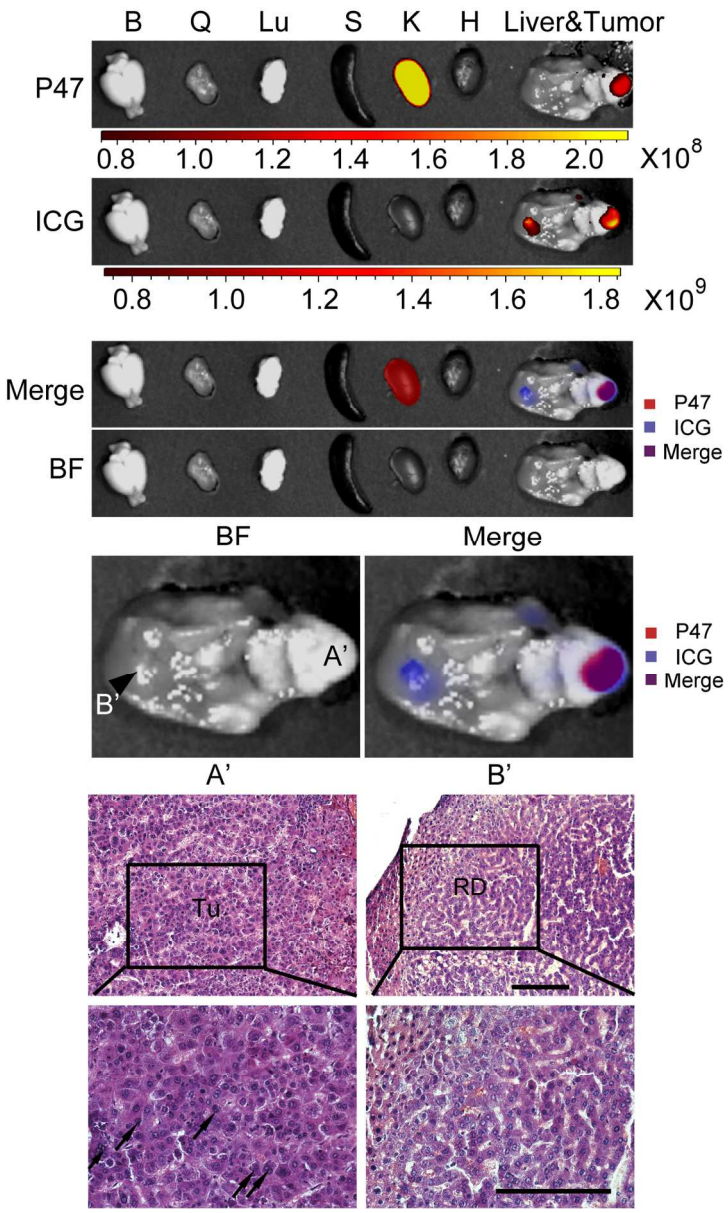

(C) Fluorescence signal distribution of AF680-labeled P47 and ICG in DENA-induced autochthonous HCC mice. Wide black arrowhead (B') points to regenerative nodules (RD); A' refers to tumor in which narrow black arrows point to binuclear tumor cells.

108x180mm (300 x 300 DPI)

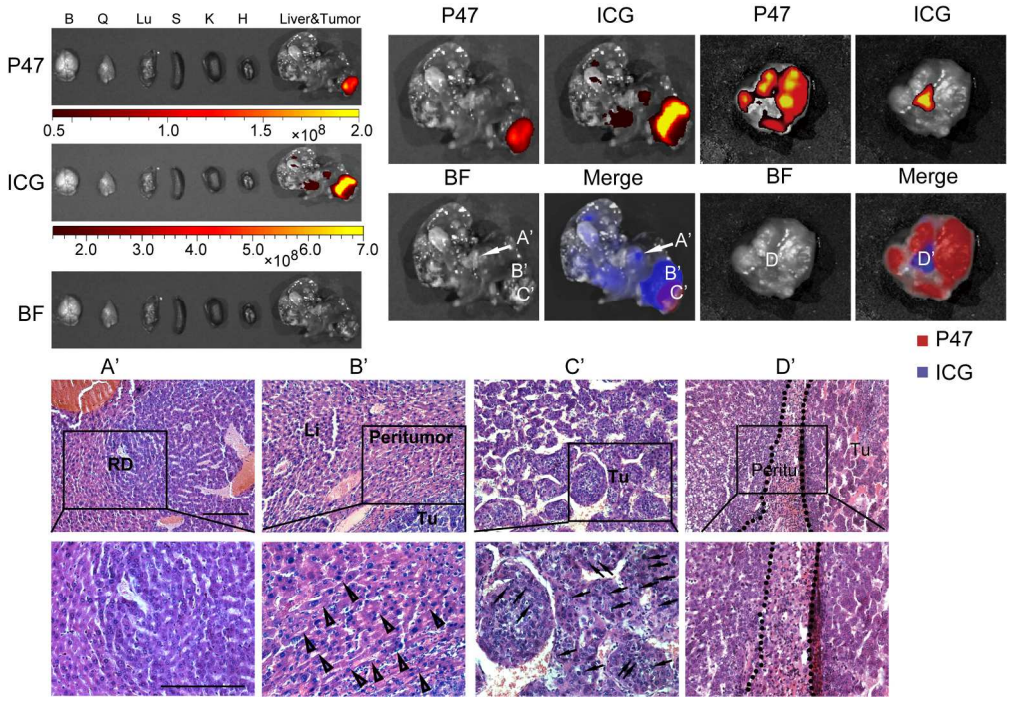

(D) Fluorescence signal distribution of AF680-labeled P47 and ICG in DENA-induced autochthonous HCC mice with more binuclear tumor cells. White arrow points to the regenerative nodule (RD) (A'); Tu –Tumor. B' and D' refer to areas containing more compressed liver cells with elongated and flat shapes. Wide black arrowheads point to compressed liver cells. C' represents the HCC tumor in which narrow black arrows point to binuclear tumor cells.

198x137mm (300 x 300 DPI)

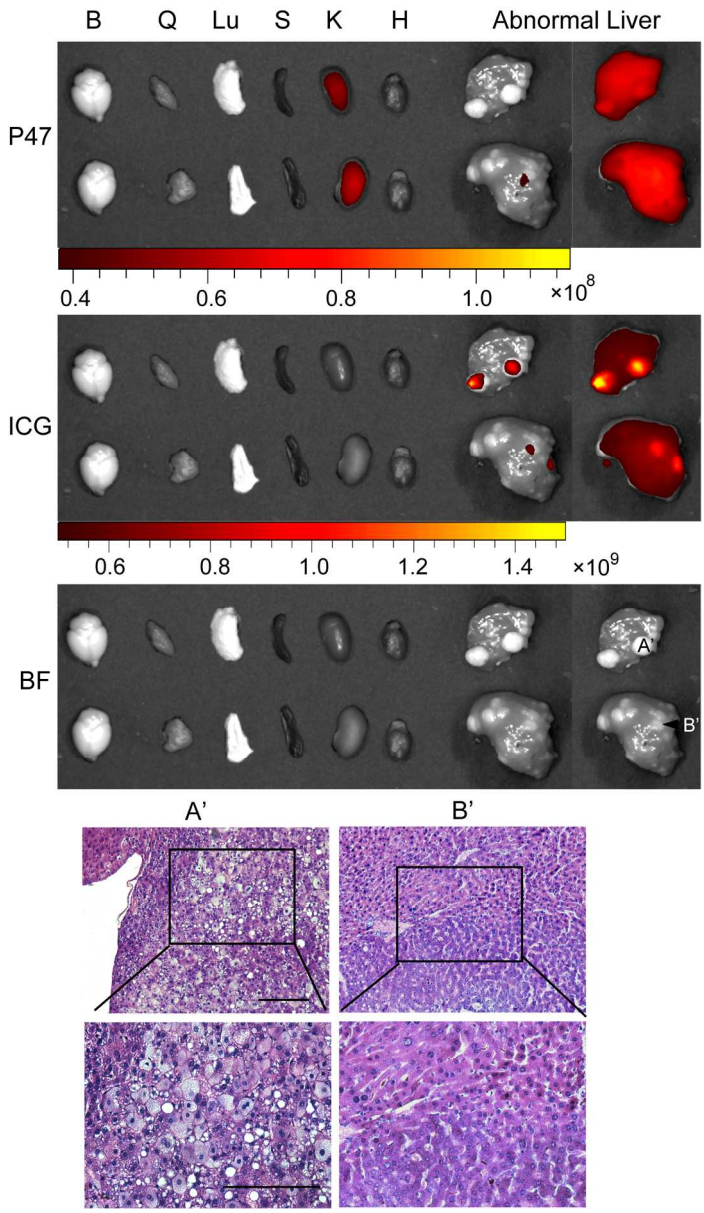

(E) Fluorescence signal distribution of AF680-labeled P47 and ICG in DENA-induced mice bearing hepatic hyperplasia. A' refers to areas with ballooning degeneration; B' represents regenerative nodules (RD).

117x203mm (300 x 300 DPI)

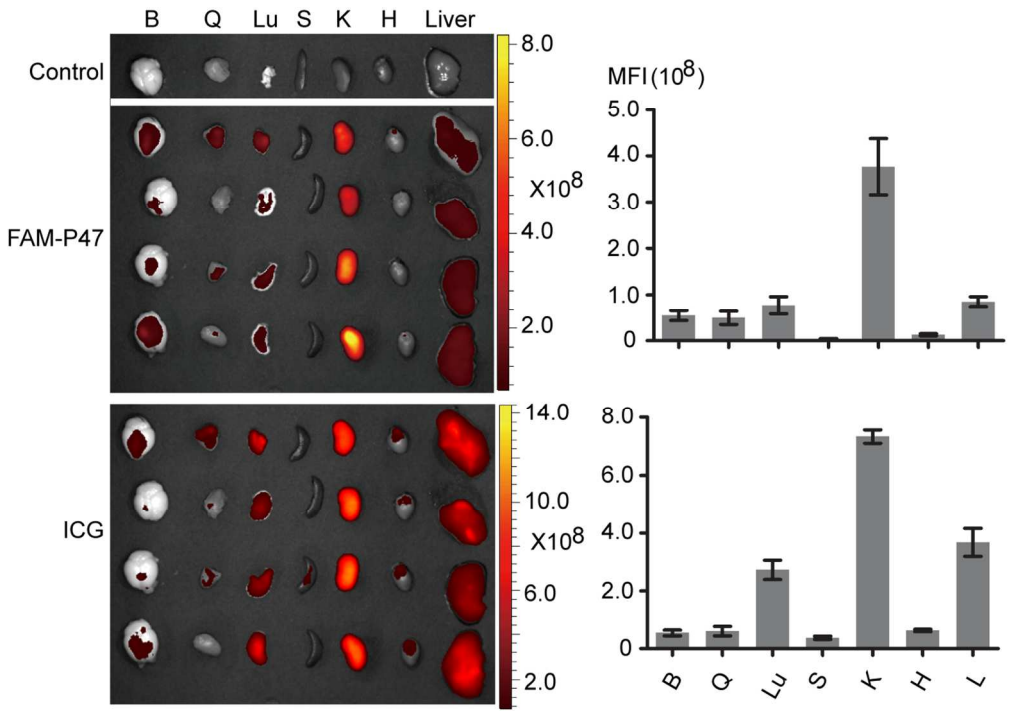

(F) Tissue distribution of FAM-labeled P47 and ICG in normal C57BL/6 mice (n=3). B-brain; Q-quadriceps; Lu- lung; S-spleen; K-kidney; H-heart.

120x84mm (300 x 300 DPI)

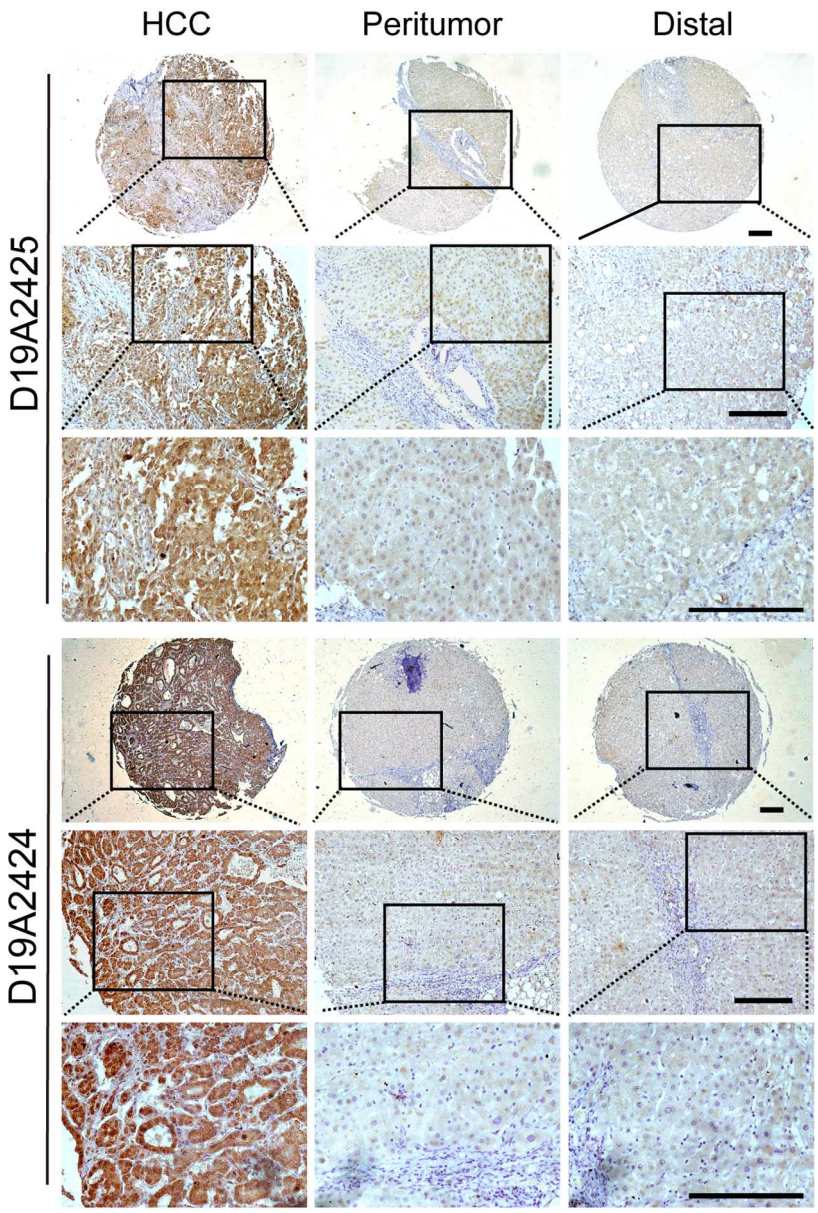

Figure 6. Investigation on the capability of P47 in differentiating HCC from peritumoral regions in HCC patient tissues. (A) Immunohistochemical staining of FLAG-tagged P47 in HCC patient tissue arrays. Distal – distal region. FLAG antibody was used to detect the distribution of FLAG-tagged P47 in different HCC patient tissues. D19A2425 and D19A2424 refer to the code for patient tissues.

105x156mm (300 x 300 DPI)

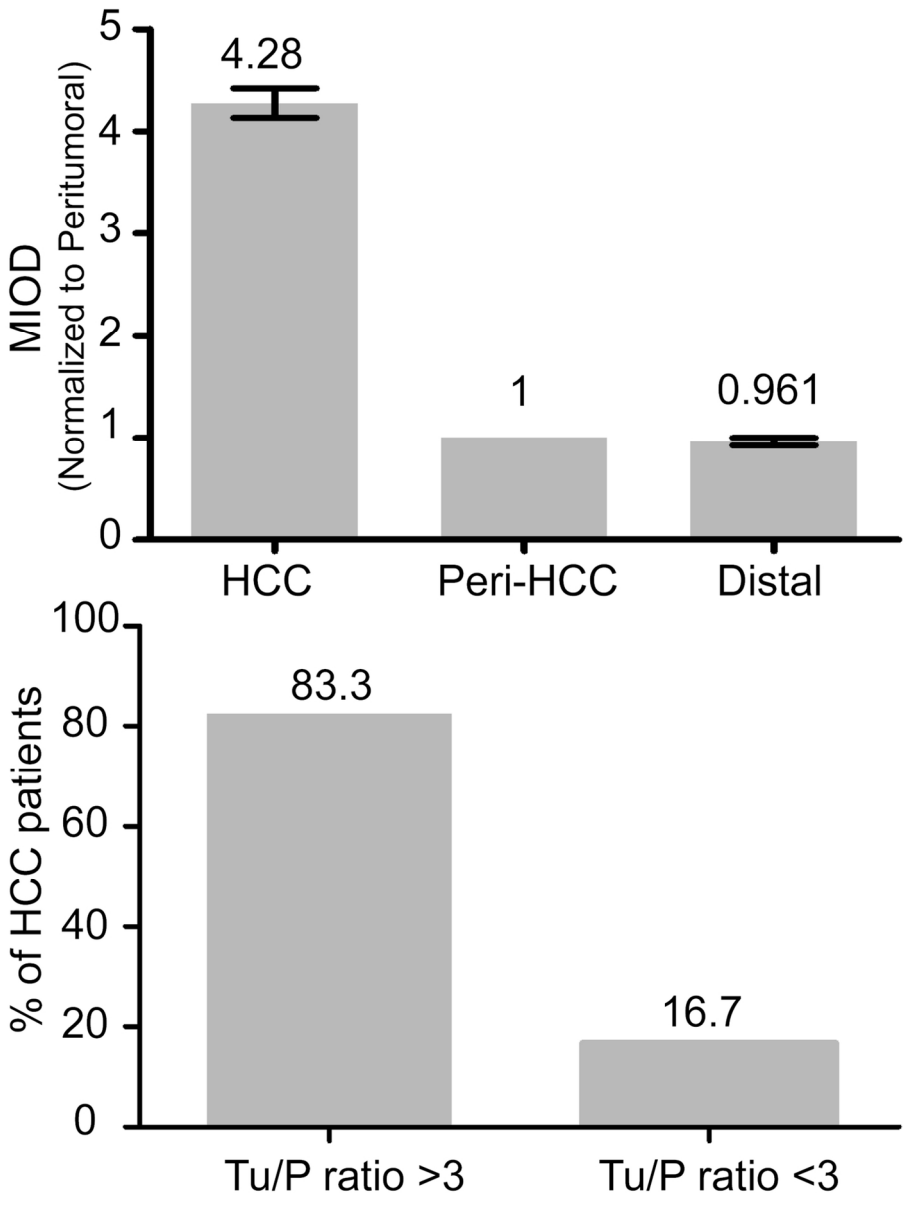

(B) Quantitative analysis of staining signal intensity in different HCC patient tissues and percentage of HCC patients with different Tu/P ratios. The data was presented as MIOD (Mean Integrated Optical Density) after normalized to peritumoral tissues (HCC, n=102; peritumoral tissue, n=102; distal region, n=30). Tu/P refers to Tumor/ peritumoral regions.

119x159mm (300 x 300 DPI)

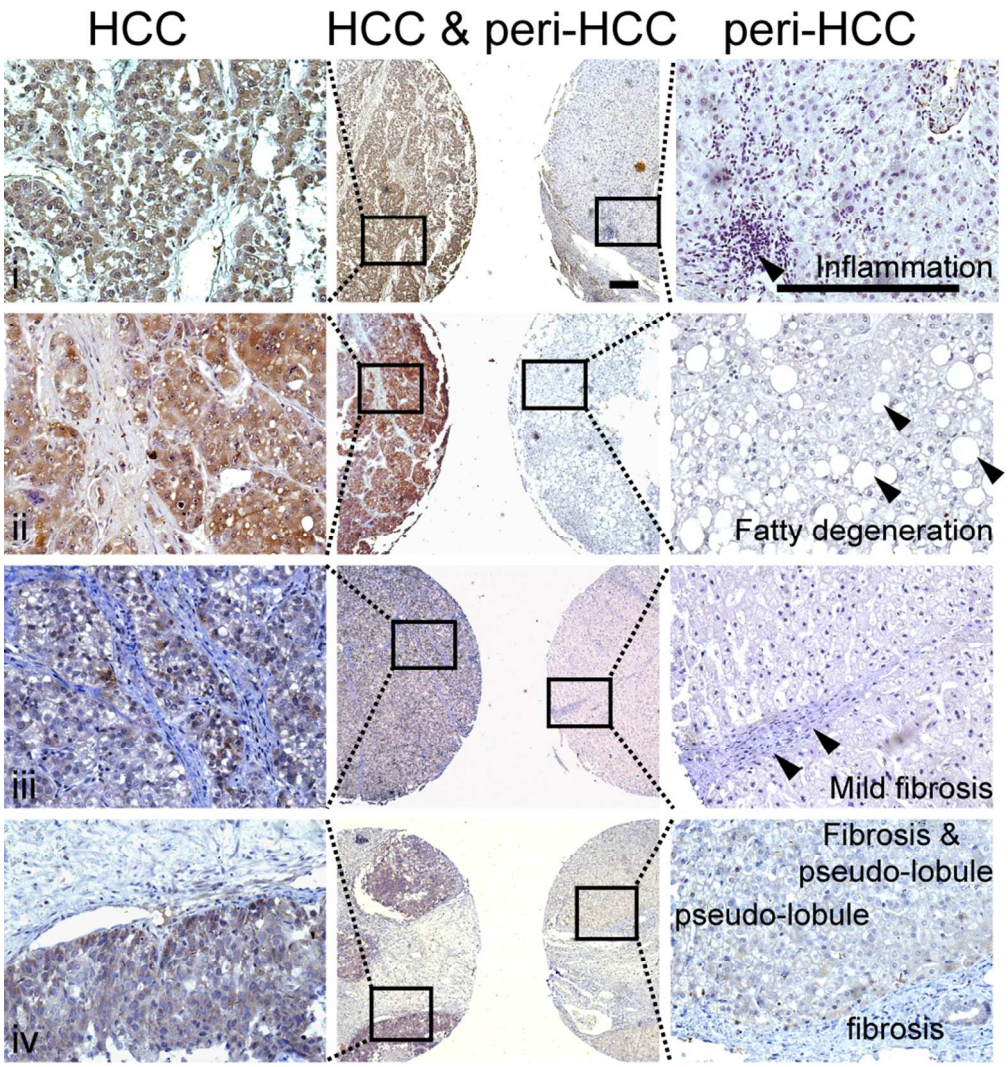

(C) Immunohistochemical staining of FLAG-tagged P47 in HCC patient tissues containing heterogeneous background liver. In (i) the arrowhead points to inflammation; (ii) arrowheads point to fatty degeneration areas; (iii) liver fibrosis.

90x96mm (300 x 300 DPI)

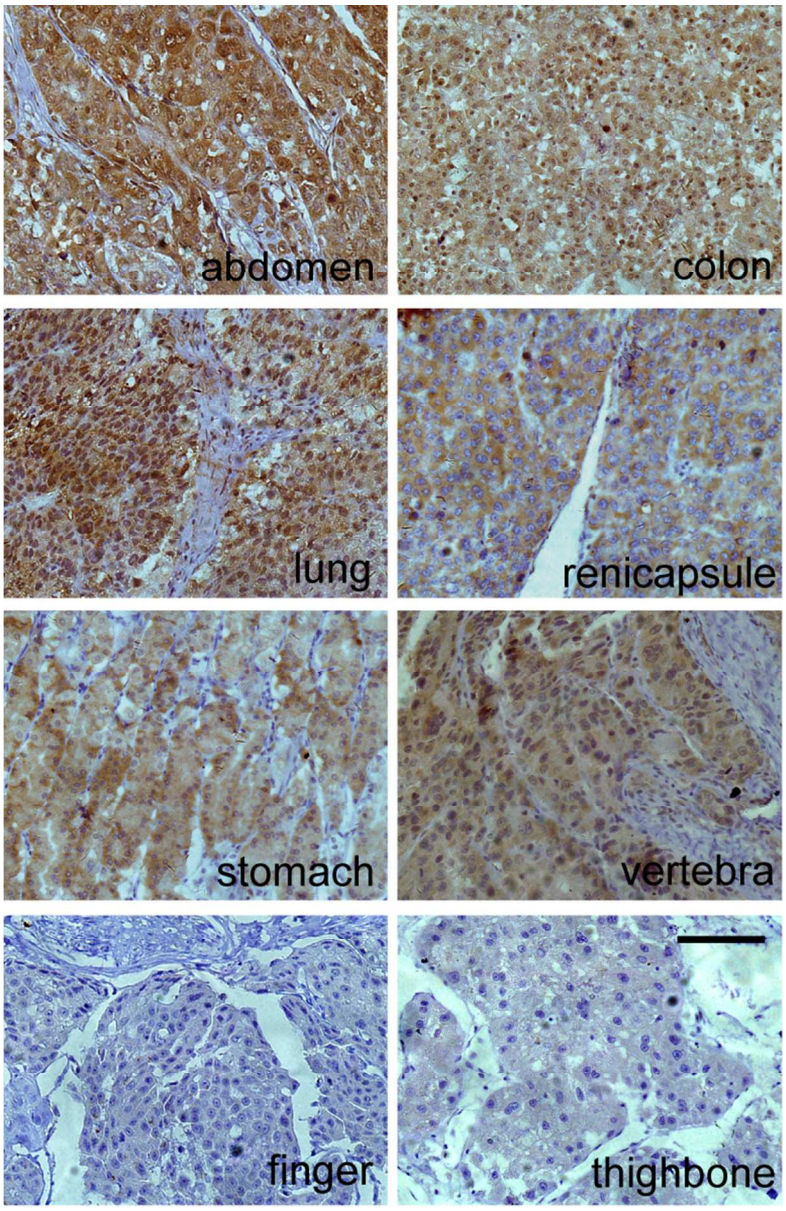

(D) Immunohistochemical staining of FLAG-tagged P47 in HCC patient tissues containing metastasis.

65x100mm (300 x 300 DPI)

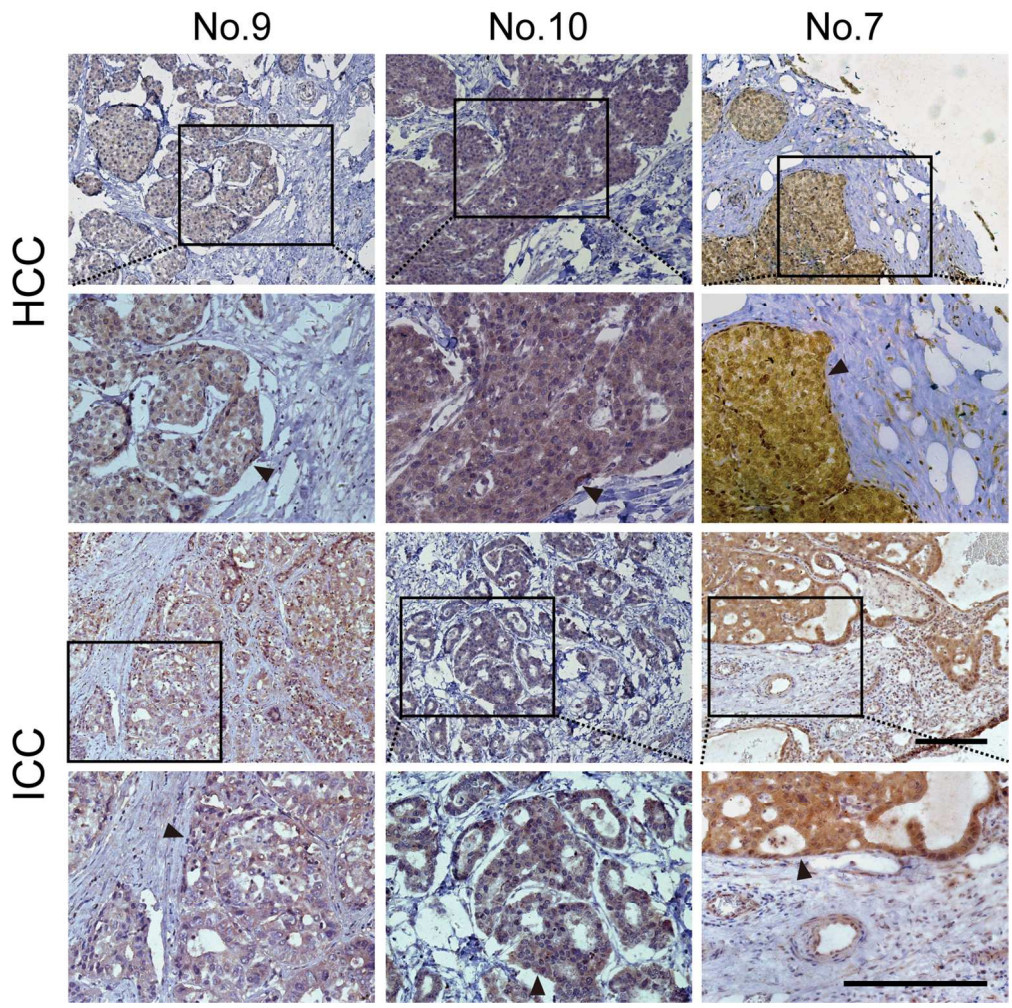

(E) Immunohistochemical staining of FLAG-tagged P47 in combined HCC and intrahepatic-cholangiocarcinoma (ICC) patient tissues (scale bar=100 μm). The arrowheads point to the margin between tumor and peri-tumor.

130x129mm (300 x 300 DPI)

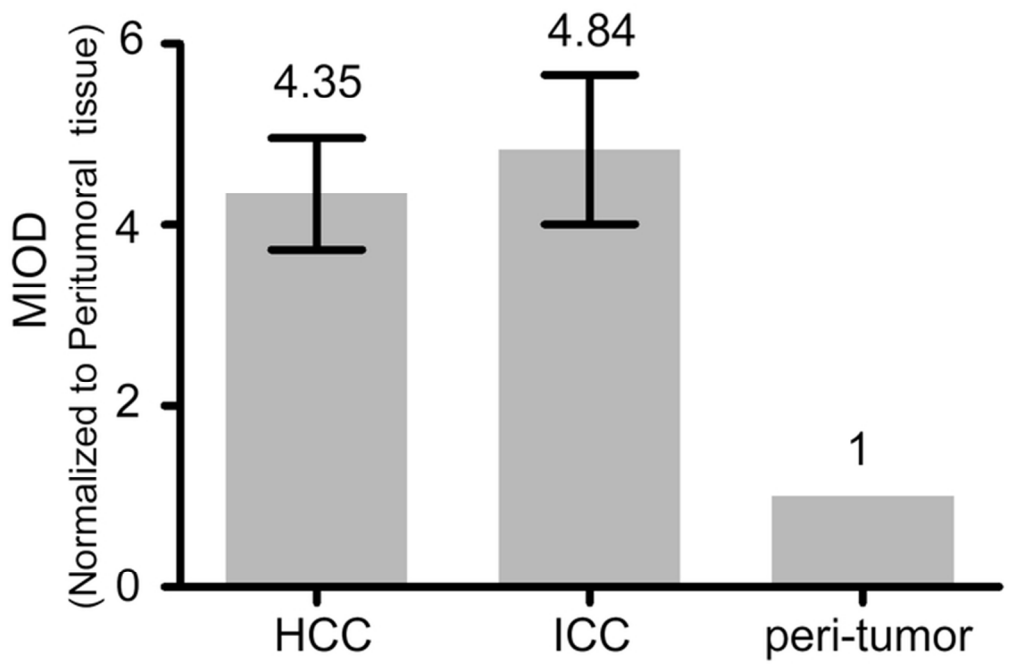

(F) Quantitative analysis of staining signal intensity in different HCC and ICC patient tissues. The data was presented as MIOD after normalized to peritumoral tissues (HCC, n=12; ICC, n=10; peritumoral tissues, n=12; error bars are + SEM).

61x40mm (300 x 300 DPI)

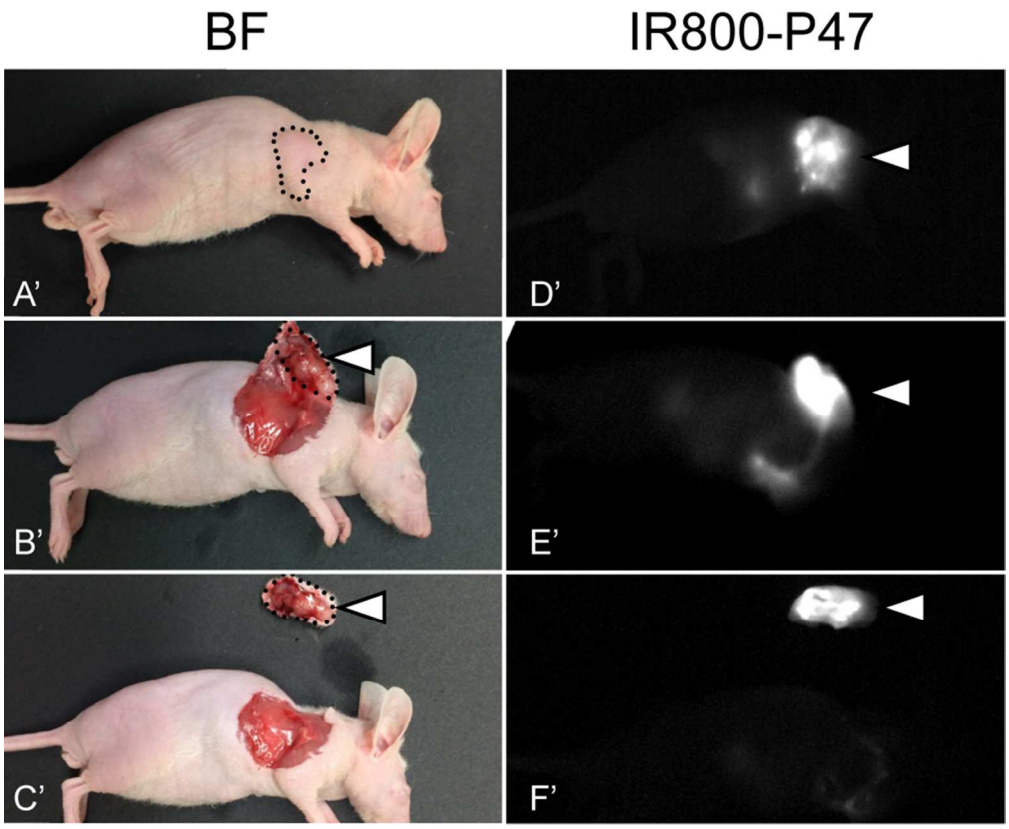

Figure 7. Assessment of IR800-labeled P47 peptide in fluorescence-guided surgery. IR800-labeled P47 (0.5 mg/kg) was injected intravenously into ectopic or orthotopic LM3 HCC mice 24 h prior to surgery. (A) IR800-labeled P47 guided surgery in ectopic HCC mice. A' and D' show the tumor prior to surgery; B' and E' refer to the tumor during surgery; C' and F' indicate the tumor after surgery. White arrowhead points to the ectopic tumor.

81x67mm (300 x 300 DPI)

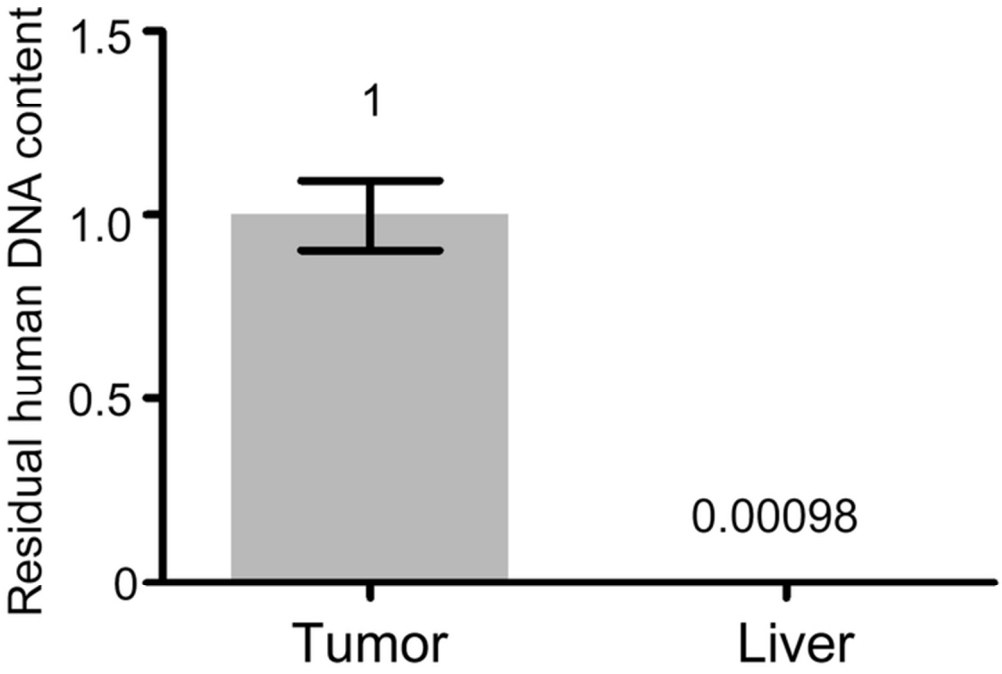

(B) Quantitative analysis of residual human DNA content with real-time quantitative PCR to verify the completeness of surgery (n=3).

61x41mm (300 x 300 DPI)

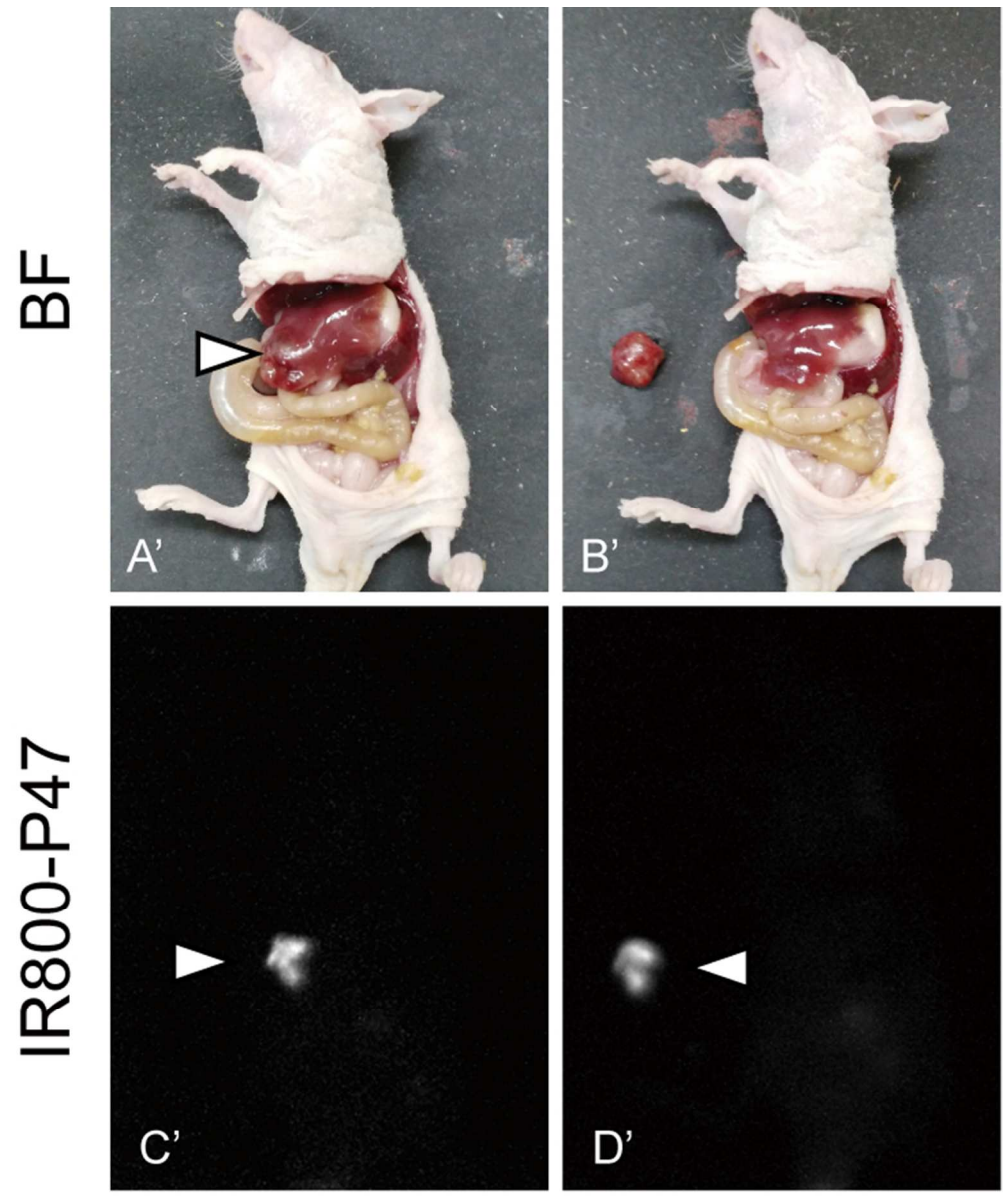

(C) IR800-labeled P47 guided surgery in orthotopic HepG2 HCC mice bearing focal and solitary tumors. A' and C' show the tumor prior to surgery; B' and D' indicate the tumor after surgery. White arrowhead points to the orthotopic tumor.

61x74mm (300 x 300 DPI)

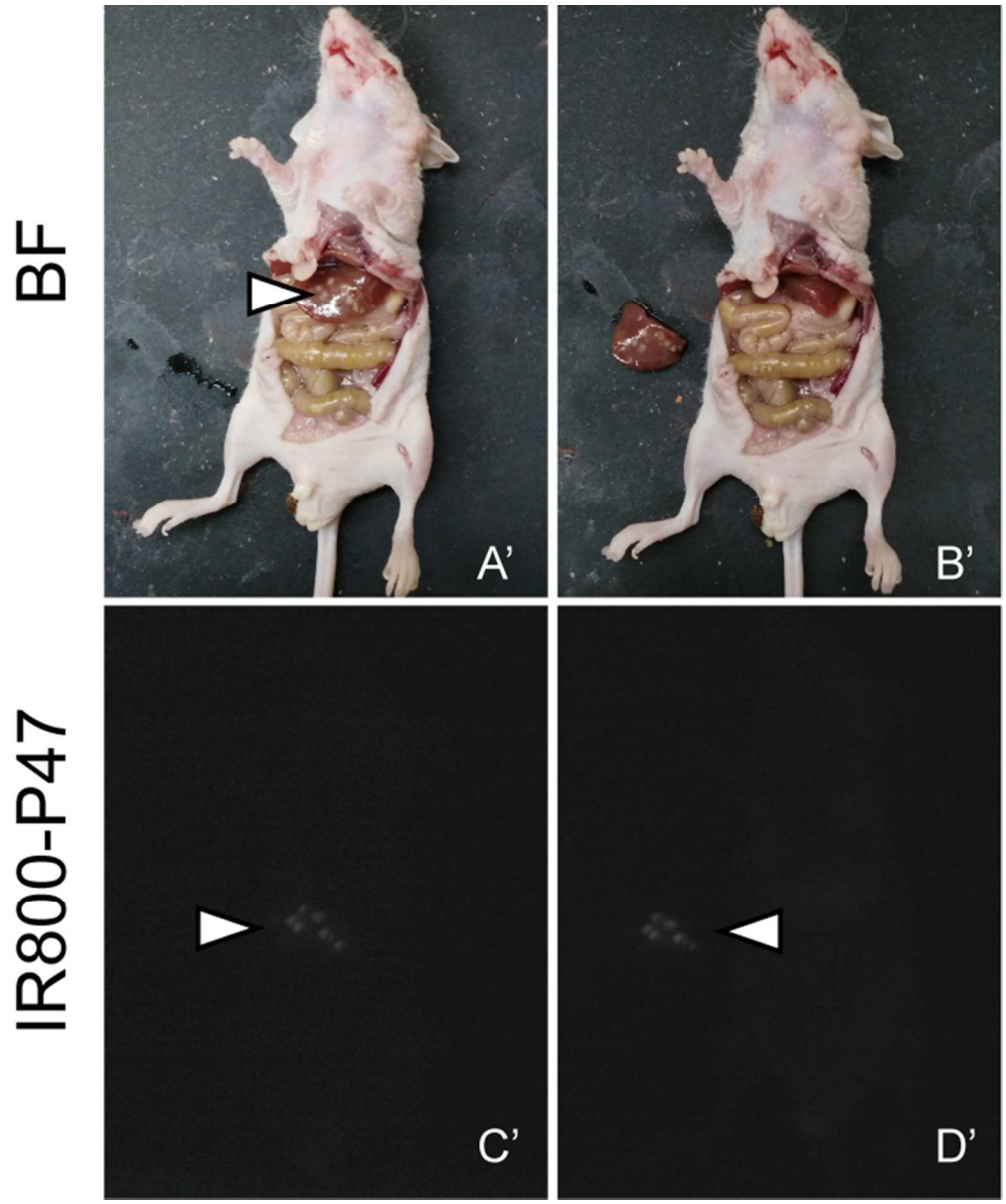

(D) IR800-labeled P47 guided surgery in orthotopic LM3 HCC mice bearing multinodular and dispersed micronodules. A' and C' show the tumor prior to surgery; B' and D' indicate the tumor after surgery. White arrowhead points to the orthotopic tumor.

61x73mm (300 x 300 DPI)

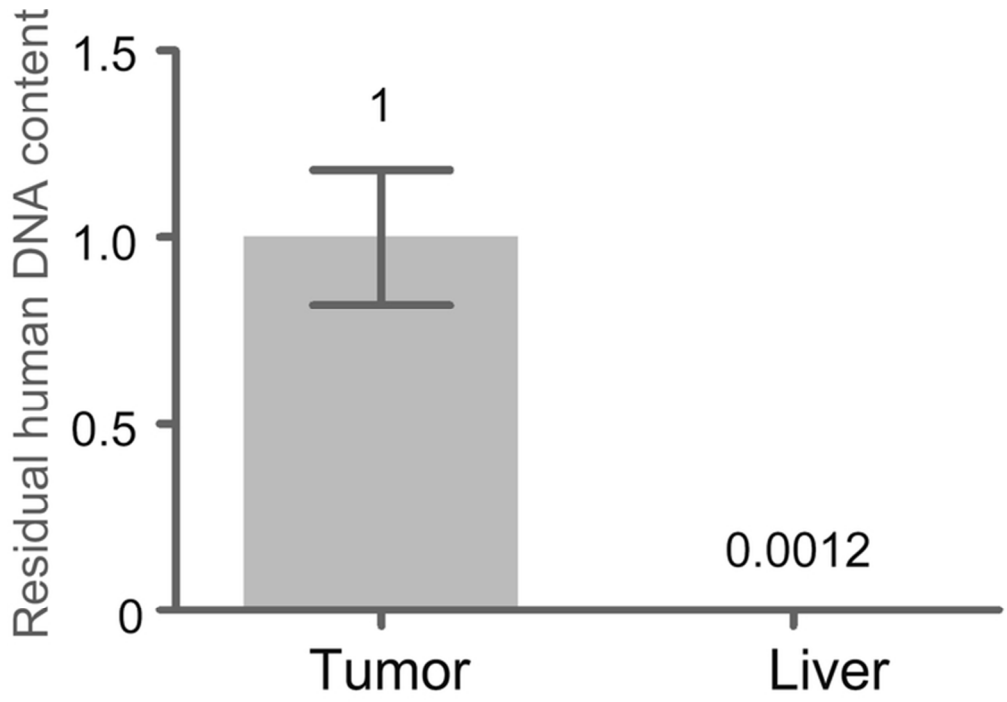

(E) Quantitative analysis of residual human DNA content with real-time quantitative PCR to verify the complete removal of micronodules (n=3).

61x43mm (300 x 300 DPI)